TU Delft

Delft University of Technology

Document Version
Final published version

Citation (APA)
Meng, Z., Liu, Q. F., Ukrainczyk, N., Mu, S., Zhang, Y., & De Schutter, G. (2023). Numerical study on the chemical and electrochemical coupling mechanisms for concrete under combined chloride-sulfate attack. *Cement and Concrete Research*, *175*, Article 107368. https://doi.org/10.1016/j.cemconres.2023.107368

Important note
To cite this publication, please use the final published version (if applicable).
Please check the document version above.

Copyright
In case the licence states “Dutch Copyright Act (Article 25fa)”, this publication was made available Green Open Access via the TU Delft Institutional Repository pursuant to Dutch Copyright Act (Article 25fa, the Taverne amendment). This provision does not affect copyright ownership.
Unless copyright is transferred by contract or statute, it remains with the copyright holder.

Sharing and reuse
Other than for strictly personal use, it is not permitted to download, forward or distribute the text or part of it, without the consent of the author(s) and/or copyright holder(s), unless the work is under an open content license such as Creative Commons.

Takedown policy
Please contact us and provide details if you believe this document breaches copyrights.
We will remove access to the work immediately and investigate your claim.

This work is downloaded from Delft University of Technology.

Green Open Access added to TU Delft Institutional Repository

'You share, we take care!' - Taverne project

https://www.openaccess.nl/en/you-share-we-take-care

Otherwise as indicated in the copyright section: the publisher is the copyright holder of this work and the author uses the Dutch legislation to make this work public.

Cement and Concrete Research 175 (2024) 107368

Contents lists available at ScienceDirect

Cement and Concrete Research

journal homepage: www.elsevier.com/locate/cemconres

Numerical study on the chemical and electrochemical coupling mechanisms for concrete under combined chloride-sulfate attack

Zhaozheng Meng [a,g], Qing-feng Liu [a,b,*], Neven Ukrainczyk [c], Song Mu [d], Yufei Zhang [e], Geert De Schutter [f]

[a] State Key Laboratory of Ocean Engineering, School of Naval Architecture, Ocean and Civil Engineering, Shanghai Jiao Tong University, Shanghai, China
[b] Shanghai Key Laboratory for Digital Maintenance of Buildings and Infrastructure, Shanghai, China
[c] Institute of Construction and Building Materials, Technical University of Darmstadt, Franziska-Braun-Str 7, 64287 Darmstadt, Germany
[d] State Key Laboratory of High Performance Civil Engineering Materials, Jiangsu Research Institute of Building Science, Nanjing, China
[e] Department of Civil and Environmental Engineering, Faculty of Science and Technology, University of Macau, Macau
[f] Ghent University, Department of Structural Engineering and Building Materials, Magnel-Vandepitte Laboratory, Technologiepark-Zwijnaarde 60, 9052 Ghent, Belgium
[g] Microlab, Faculty of Civil Engineering and Geosciences, Delft University of Technology, 2628 CN, Delft, The Netherlands

ARTICLE INFO

Keywords:
Chloride ingress
Sulfate attack
Competitive binding
Electrostatic potential
Numerical modelling
Reactive-transport

ABSTRACT

Cementitious materials exposed to marine and saline environments are commonly threatened by a combined attack of sulfate and chloride ions. This study developed a numerical framework to investigate two combined coupling mechanisms of 1) coupled solid-liquid chemical reactions for competitive chloride-sulfate attack and 2) electrostatic multi-ion coupling effect on reactive-transport mechanisms. Various chemical reactions including sulfate attack with anhydrous calcium aluminates, secondary precipitation of expansive minerals, competitive binding, and calcium leaching have been quantified. The electrostatic potential caused by multi-ions coupling was solved according to constitutive electrochemical laws. After model validation, the chemical coupling mechanisms for solid-liquid reactions during competitive chloride-sulfate binding were investigated. On this foundation, the influence of electrostatic multi-ionic coupling effects on ionic transport and its interaction with chemical coupling were disclosed. It was found that neglecting multi-ions coupling effect would result in an underestimated chemical coupling strength in competitive chloride-sulfate binding.

1. Introduction

Nowadays, cementitious materials have been widely applied in reinforced concrete (RC) structures to build human-made infrastructure environment (e.g., large buildings, bridges, dams, road and waste water networks etc.). Concrete is by far the most used material due to its preferred workability and mechanical properties at low economic and environmental costs [1–4]. However, when exposed to marine and saline environments, cement-based materials are typically susceptible to aggressive substances such as chloride and sulfate ions which limit concrete durability and structural service life, due to steel corrosion and concrete deterioration respectively [5–7]. Moreover, combined ingress of external ions from environment and leaching of internal ions from the concrete (pore solution) outwards may have significant effects on the two degradation processes. Consequently, in order to predict the service life more reliably and ensure working safety of existing RC structures, it requires more understanding of the underlying deterioration mechanisms for cementitious materials. In particular, the coupling from the simultaneous attack of chloride and sulfate ions has recently attracted increasingly more scientific attention but remained as one of the key challenges for concrete durability [8–10].

The individual mechanisms for chloride induced reinforcement corrosion and sulfate induced damage of cement matrix have been well studied [11–13]. The penetrated chloride ions will accumulate at embedded steel surface, and initiate depassivation and polarization of reinforcement [14–16]. After initiation of steel corrosion, expansive corrosion products are formed by a series of electrochemical reactions where the availability of moisture, oxygen and chloride play a critical role [17–19]. Apart from depassivation, chlorides can diffuse through steel corrosion layer and cancel the charge polarization near metal

* Corresponding author at: State Key Laboratory of Ocean Engineering, School of Naval Architecture, Ocean and Civil Engineering, Shanghai Jiao Tong University, Shanghai, China.
E-mail address: liuqf@sjtu.edu.cn (Q.-f. Liu).

https://doi.org/10.1016/j.cemconres.2023.107368
Received 8 March 2023; Received in revised form 18 October 2023; Accepted 30 October 2023
Available online 24 November 2023
0008-8846/© 2023 Elsevier Ltd. All rights reserved.

surface to further catalyze steel corrosion rate [20,21]. The progressive expansion of corrosion products cause cracking and even spalling of concrete cover, which will in turn exacerbate the chloride ingress [22–24].

As for the cement matrix degradation induced by external sulfate attack (ESA), researchers have found that sulfate ions react with hydrated cement phases to form expansive products such as gypsum and Ettringite, which will eventually cause overall expansion and cracking of cement matrix [25–27]. For cementitious materials exposed to the dual attack of sulfate and chloride ions, those two ions will competitively react with hydration products, making the degradation process even more complex [28,29]. In addition to the interaction with chloride ingress, the chemical reactions caused by external sulfate attack also involve dissolution of calcium-bearing phases in hydrated cement system, which will further aggravate degradation of the mechanical properties as well as facilitate the ingress of deleterious substances such as chloride, sulfate, moisture and oxygen [30–32].

With regard to concrete suffering from the combined chloride-sulfate attack, which is commonly observed in practice, various experimental studies have been carried out to study the intrinsic degradation mechanisms. Dehwah et al. [33] investigated the steel corrosion under the coexistence of chloride and sulfate ions, and they found that the concomitant presence of sulfate ions could increase the corrosion rate but contributed little to the advancement of corrosion initiation. Shaheen and Pradhan [34] studied the effect of cation type and found that compared to sodium sulfate, magnesium sulfate would lead to higher corrosion rate of reinforcing steel in concrete. In addition to the influence of sulfates on chloride-induced steel corrosion, the ageing of the cement matrix under simultaneous exposure to chloride and sulfate ions are also studied in detail [35–37]. An experimental program conducted by Chen et al. [28] reported that the co-existence of sulfate ions could retard the chloride ingress and the formation of Friedel's salt for ordinary Portland cement. However, experimental results presented by Cao et al. [38] revealed that the influence of sulfate ion on chloride penetration was time-dependent, and a short-term exposure could accelerate chloride diffusion by decomposing previously formed Friedel's salt. More recently, Zhao et al. [39] found that concrete exposed to the mixed solution of sulfate and chloride suffered from more serious strength loss compared to the individual actions of each ion, in agreement with results from Wang et al. [40].

Apart from the abovementioned experimental studies, both the individual and combined attack of chloride and sulfate ions have been systematically studied by numerical modelling approach. Based on the modified Fick's second law, numerous models for chloride and sulfate ions ingress in concrete have been developed [41,42]. Furthermore, in the light of works by Marchand and Samson et al. [43,44], reactive transport model has been widely adopted to model the interactive relationships among deleterious ions and hydrated cement system [45]. Qin et al. [46] established the diffusion reaction model with a further consideration of calcium leaching to study the individual external sulfate attack, and results indicated that calcium leaching and sulfate-induced degradation had a mutual stimulation effect. Zhang et al. [47] developed a numerical model to quantify the influence of external sulfate attack on chloride diffusivity and binding capacity. They found that chloride binding capacity declined about 18 % in combined chloride-sulfate environment, while the chloride diffusivity in the sulfate damaged zone increased (5– 10 times) with the sulfate-induced damage evolution, but in the sulfate non-damaged zone it decreases due to the pore-refining process. Furthermore, Wang et al. [48,49] simulated the combined chloride-sulfate attack from the perspective of reaction kinetics, and it turned out that the highest content of bound chloride ion appeared at a more inward position along concrete cover depth due to the ingress of sulfate ions. Most recently, Chen et al. [50,51] proposed a series of numerical models to investigate the time and spatial development of the interaction between chloride and sulfate ions, and other influence factors such as curing time. However, the multi-ions coupling effect and electric field induced by charge imbalance in pore solution were not considered by these models. By adopting the advancement in geochemistry and thermodynamic modelling techniques, numerical models have also been developed to a wider implementation range for predicting chloride and sulfate induced degradation of cementitious materials from the perspective of chemical equilibrium assumption [52–54].

According to the preceding literature review, it can be seen that remarkable progress has been made by previous studies. However, the combined chloride-sulfate attack is coupled with solid-liquid chemical reactions such as expansive minerals precipitation, competitive adsorption and calcium leaching, while very few studies have integrated those internally coupled reactions into one model and further discuss the influencing mechanisms. In addition to the chemical coupling relationships among solid-liquid chemical reactions, electrostatic multi-ion coupling effect induced by the concomitant existence of other ionic species in concrete pore solution was also less concerned in previous studies. The electrostatic potential induced by the ionic charge imbalance inside concrete pore solution will not only influence the ionic transport behavior, but also exert an effect on the coupled solid-liquid chemical reactions for chloride-sulfate attack, which will further change the competitive binding intensity. Therefore, it can be found that there existed two combined coupling processes during the chloride-sulfate attack (i.e., the chemical reactions coupling and multi-ionic coupling), which need to be highlighted in the coming studies.

To clarify the relationships between the chemical and electrochemical coupling phenomena (i.e., solid-liquid chemical reactions coupling and electrostatic multi-ionic coupling), the following work will be carried out in this study to fill the abovementioned research gap. Firstly, based on the reaction kinetics of hydrated cement phases with sulfate and chloride ions, as well as the solid–liquid relation of calcium-bearing phases, a reactive transport model will be established. The interactions between chloride and sulfate ions, and the mutual stimulation relationship between calcium leaching and sulfate erosion have been reflected. The coarse aggregates intrusion in cement bulk and existence of ITZ have also been taken into account. In addition, the multi-ions coupling effect and electrostatic potential induced by ionic charge imbalance are quantitively characterized following the constitutive electrochemical laws. Meanwhile, the porosity evolution and ionic diffusivity variation caused by the dissolution of calcium-bearing phases and precipitation of expansive products due to external sulfate attack have also been taken into account. Validated by the experimental data, the ionic concentrations, cement chemical compositions and porosity variation under combined chloride-sulfate attack will be firstly discussed. Then, based on the coupled solid-liquid chemical reactions, the competitive chloride-sulfate binding mechanisms are quantitively analyzed, and the influence factors of the competitive intensities are also investigated. On this basis, by comparing cases with and without the consideration of multi-ionic coupling effect, the influence of electrostatic coupling effect on ionic transport and competitive chloride-sulfate binding intensity are discussed, and interactions between these two coupling processes are revealed. Finally, new findings which have not been reported in previous studies are highlighted. The presented numerical model is hoped to better understand the underlying mechanisms and provide an effective approach to predict the degradation process for concrete exposed to the synergetic chloride-sulfate attack.

2. Model establishment

Fig. 1 illustrates the schematic diagram for concrete under the combined chloride-sulfate attack. For reinforced concrete structures exposed in marine and saline environments, chloride and sulfate ions are typical harmful ions, which will result in the corrosion of embedded reinforcement and damage of concrete. From a more microscopic point of view, as shown in the bottom of Fig. 1, sulfate and chloride ions originating from a harsh external environment and penetrate into

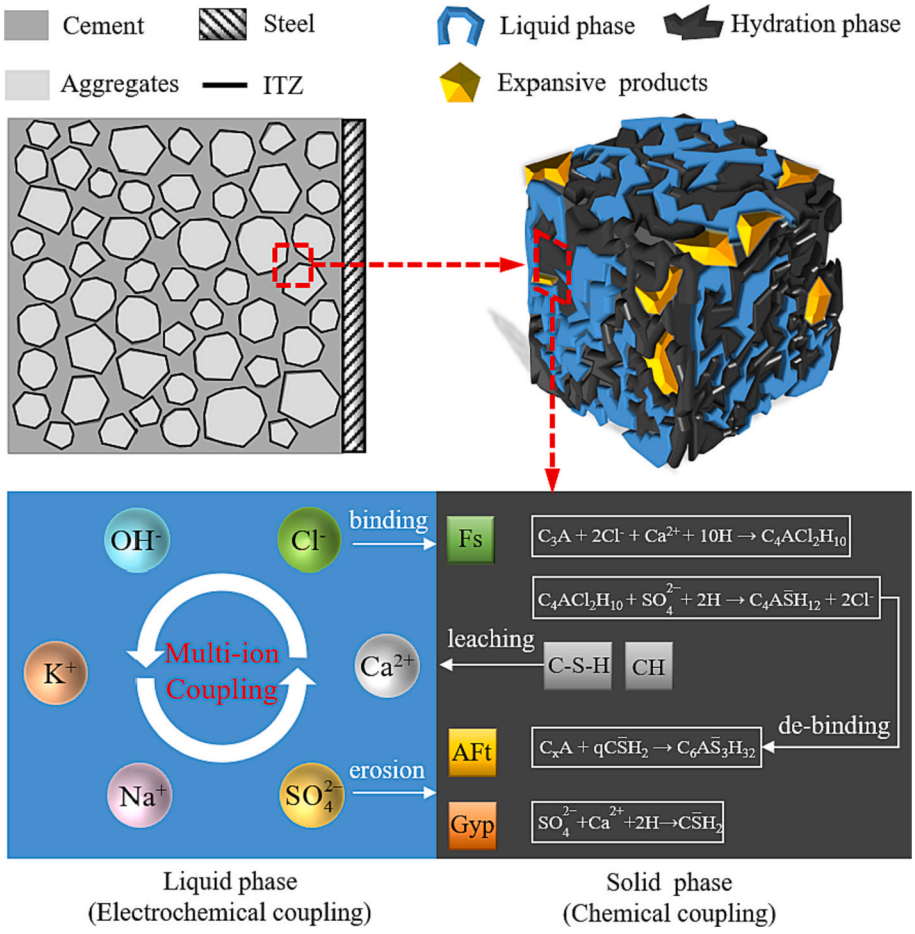


Fig. 1. Schematic diagram of mechanisms for concrete under combined chloride-sulfate attack from the perspective of meso-scale modelling, solid-liquid chemical reactions and multi-ion (electrostatic) coupling.

concrete by a reactive-transport mechanism, and a series of chemical reactions between hydrated cement products and pore solutions will occur in a coupled manner. On the one hand, free chloride ions will react with hydrated compounds (e.g., to form Friedel's salt and physically bind on their surfaces). On the other hand, sulfate ions will also competitively react with hydrated cement compounds such as portlandite and mono-sulfates to form expansive products like Gypsum and Ettringite. Simultaneously, the penetrated sulfate ions will also react with precipitated Friedel's salt to release previously bounded chloride ions and precipitate sulfates. The expansive products firstly fill capillary pores leading to a reduced diffusivity [55], but the subsequent expansion stress may also cause cracking of cement matrix. However, contrary to the voids filling caused by expansive products, due to the consumption of calcium ions required by the abovementioned reactions and leaching out of the concrete, calcium ions are continuously being released from the calcium-bearing phases, which will contribute to a decreased solid volume. In addition to the chemical reactions, the electrochemical coupling effect also exists. Because of the differences in transport properties and charges carried by various ions, an electrostatic potential will be generated in concrete pore solution, which will further affect the ionic transport behavior and solid-liquid chemical reactions [56]. Consequently, the influence of electrostatic coupling effect during the combined chloride-sulfate attack also needs considerable attentions.

2.1. Solid products precipitation by ESA

When external sulfate ions ingress into cementitious materials, a series of chemical reactions occur which are referred as the deterioration process caused by ESA [57]. In this study, the source of sulfate ions is selected as a sodium sulfate solution while the effect of different cation types on chemical reactions is not included. Therefore, secondary gypsum ($C\bar{S}H_2$) crystals are initially formed by the chemical reaction between sulfate and calcium ions that also partly originate from calcium hydroxide (CH) and calcium silicate hydrates (C-S-H).

$$SO_4^{2-} + Ca^{2+} + 2H \rightleftarrows C\bar{S}H_2 \quad (1)$$

The precipitated secondary gypsum (or more precisely the sulfate ions in the pore solution, according to the solubility product K_{sp}) reacts with hydrated and unreacted calcium aluminate to form Ettringite ($C_4A\bar{S}_3H_{32}$), which can be simplified by Eqs. (2)–(4). More detailed chemical thermodynamic description of the solid-liquid solubility equilibrium is not considered here, to avoid high computational costs in rigorous reactive-transport models, thus providing a simplified (governing) mass balance and time-dependent reaction kinetics modelling in a meso-scale, namely by explicitly being able to also consider concrete aggregates effects and mechanical effects. Moreover, it should be noted that due to the low reaction rate between tetracalcium aluminoferrite (C_4AF) and gypsum, the corresponding reaction is not considered [58], and only three calcium aluminate phases are considered here, that is, anhydrated tricalcium aluminate (C_3A), and two AFm hydrates tetracalcium aluminate (C_4AH_{13}) and mono-sulfate ($C_4A\bar{S}H_{12}$).

$$C_3A + 3C\bar{S}H_2 + 26H \rightleftarrows C_6A\bar{S}_3H_{32} \quad (2)$$

$$C_4AH_{13} + 3C\bar{S}H_2 + 14H \rightleftarrows C_6A\bar{S}_3H_{32} + CH \quad (3)$$

$$C_4A\bar{S}H_{12} + 2C\bar{S}H_2 + 16H \rightleftarrows C_6A\bar{S}_3H_{32} \quad (4)$$

Based on previous studies by Tixier [59], the chemical reactions between gypsum and calcium aluminate phases can be integrated in the lumped form as

$$C_xA + qC\bar{S}H_2 \rightarrow C_6A\bar{S}_3H_{32} \quad (5)$$

where C_xA represents the equivalent grouping of calcium aluminate phases, and can be determined as $C_xA = \sum_{i=1}^{3}\lambda_i C_i$; λ_i represents the molar fraction of the reacted calcium aluminate phases and can be calculated as $\lambda_i = C_i/\sum_{i=1}^{3}C_i$; C_i represents the molar concentration of calcium aluminate phases (mol/m^3); q represents the stoichiometric coefficient of the lumped reaction and can be determined as $q = 3\lambda_1 + 3\lambda_2 + 2\lambda_3$. It should be noted that the main focus of Eq. (5) is to determine stoichiometric coefficients of the main reactants and products during external sulfate attack. Consequently, other substances such as water and calcium hydroxide are not included in the lumped form, and the equation is therefore not balanced. Meanwhile, it can be noted that in Eq. (5), the lumped reaction is considered as one-direction chemical reaction (i.e., only the positive reaction directions of chemical equilibriums shown in Eqs. (2) to (4) have been considered here). This is because under the state of external sulfate attack, the Ettringite is mainly precipitated rather than consumed, so it is reasonable to simplify these equilibriums into one-direction chemical reactions and characterize the formation of Ettringite by reaction kinetics.

According to reaction kinetic laws, Eqs. (1) and (5) could be approximated as second-order equations, and the reaction rate of sulfate ions and calcium ions consumption (due to gypsum precipitation), as well as solid anhydrous calcium aluminates dissolution and gypsum precipitation caused by ESA can be obtained as [60]:

$$\frac{\partial c_{SO_4^{2-}}}{\partial t} = -k_1 c_{SO_4^{2-}} c_{Ca^{2+}} \quad (6)$$

$$\left(\frac{\partial c_{Ca^{2+}}}{\partial t}\right)_{ESA} = -k_1 c_{SO_4^{2-}} c_{Ca^{2+}} \quad (7)$$

$$\frac{\partial C_{C_xA}}{\partial t} = -k_2 \frac{C_{C_xA} C_{gypsum}}{q} \quad (8)$$

$$\frac{\partial C_{gypsum}}{\partial t} = k_1 c_{SO_4^{2-}} c_{Ca^{2+}} - k_2 C_{C_xA} C_{gypsum} \quad (9)$$

where $c_{SO_4^{2-}}$ and $c_{Ca^{2+}}$ represent the molar concentration of sulfate ions, calcium ions in concrete pore solution (mol/m^3); C_{C_xA} and C_{gypsum} represent the solid content of equivalent grouping of calcium aluminates and gypsum (mol/m^3); k_1 and k_2 represent the reaction rate constants of Eqs. (1) and (5) respectively (obtained from [46]).

2.2. Competitive chloride-sulfate binding

In addition to the chemical reaction induced by external sulfate ingress, chloride binding should also be considered to disclose the combined chloride-sulfate attack mechanisms. As for chemical binding, chloride ions can react with the tricalcium aluminate to form Friedel's salt ($C_4ACl_2H_{10}$), as shown by Eq. (10). Besides, free chloride can also react with mono-sulfates to form Friedel's salt, as illustrated in Eq. (11). As for physical absorption, it is commonly acknowledged that the free chloride can be physically absorbed by the C-S-H gel surface, which is shown in Eq. (12) [61]. However, with the ingress of sulfate ions and local acidification caused by calcium leaching, chloride binding capacity may be reduced and previously bound chlorides are released into pore solution. In this way, counter-reactions of Eqs. (11) and (12) should be considered. Following the ionic exchange theory [62], the chemically and physically bound chloride can be determined by Eqs. (13) and (14) respectively. The reaction rate of chloride ions due to binding can be subsequently derived as the time derivative of total bound chloride concentration in Eq. (15). It should be noted that, when the concrete binding capacity is reducing and the total amount of bound chloride is decreasing, the consumption rate defined in Eq. (15) may become positive to represent the reversible release of free chloride from bound state.

$$2Cl^- + C_3A + Ca^{2+} + 10H \rightarrow C_4ACl_2H_{10} \quad (10)$$

$$2Cl^- + Ca^{2+} + C_4A\bar{S}H_{12} \rightleftarrows C_4ACl_2H_{10} + C\bar{S}H_2 \quad (11)$$

$$[C-S-H-OH] + Cl^- \rightleftarrows [C-S-H-Cl] + OH^- \quad (12)$$

$$c_{Cl^-}^{chem} = \frac{2K_{chem}c_{Cl^-}^2}{c^{SO_4^{2-}} + K_{chem}c_{Cl^-}^2} N_1 \quad (13)$$

$$c_{Cl^-}^{phy} = \frac{A_{C-S-H}K_{phy}c^{Cl^-}}{c^{OH^-} + K_{phy}c^{Cl^-}} N_2 \quad (14)$$

$$\left(\frac{\partial c_{Cl^-}}{\partial t}\right)_{binding} = -\frac{\partial\left(c_{Cl^-}^{chem} + c_{Cl^-}^{phy}\right)}{\partial t} \quad (15)$$

where $c_{Cl^-}^{chem}$ and $c_{Cl^-}^{phy}$ represent the chemically and physically bound chloride molar concentration respectively (mol/m^3); c_{Cl^-} and c_{OH^-} represent the molar concentrations for free chloride and hydroxyl ions respectively (mol/m^3); K_{chem} and K_{phy} represent the dimensionless reaction equilibrium constants for chemical reactions in Eqs. (11) and (12) respectively; N_1 represents the solid content occupied by mono-sulfates and Friedel's salt (mol/m^3); N_2 represents the molar concentration of C-S-H gel (mol/m^3); $A_{C\text{-}S\text{-}H}$ represents binding capacity per mole C-S-H gel which can be selected as 0.045 according to literature [53].

2.3. Calcium leaching

During the ingress of external sulfate and chloride ions, calcium ions leach into pore solution and out from concrete into environment according to the dissolution of CH and decalcification of C-S-H gel, increasing the porosity reducing the strength of concrete matrix, which will in turn aggravate the ESA and chloride penetration [63–65]. Therefore, taking leaching effect into consideration ensures a more accurate prediction results of chemical reactions and ionic transport behavior under the combined chloride-sulfate attack. Due to the uncertainties of chemical equilibrium mechanisms of C-S-H, it is typical to adopt the solid–liquid relation curve to depict the calcium leaching effect [66,67], which can be given as

$$c_{Ca^{2+}}^{s} = \begin{cases} C_{CSH0}\left(\frac{c_{Ca^{2+}}}{c_{Ca^{2+}}^{satu}}\right)^{\frac{1}{3}}\left(-\frac{2}{x_1^3}c_{Ca^{2+}}^3 + \frac{3}{x_1^2}c_{Ca^{2+}}^2\right) & 0 \le c_{Ca^{2+}} \le x_1 \\ C_{CSH0}\left(\frac{c_{Ca^{2+}}}{c_{Ca^{2+}}^{satu}}\right)^{\frac{1}{3}} & x_1 < c_{Ca^{2+}} < x_2 \\ C_{CSH0}\left(\frac{c_{Ca^{2+}}}{c_{Ca^{2+}}^{satu}}\right)^{\frac{1}{3}} + \frac{C_{CH0}}{\left(c_{Ca^{2+}}^{satu} - x_2\right)^3}\left(c_{Ca^{2+}} - x_2\right)^3 & x_2 \le c_{Ca^{2+}} \le c_{Ca^{2+}}^{satu} \end{cases} \quad (16)$$

where $c_{Ca^{2+}}^{s}$ is the calcium ion concentration in solid phase (mol/m^3); $c_{Ca^{2+}}^{satu}$ is the calcium ion concentration under saturated condition (mol/m^3); C_{CSH0} and C_{CH0} represent the initial molar concentration of calcium hydroxide and calcium silicate hydrates in solid phase (mol/m^3); x_1 is the calcium ion concentration in pore solution signifying the decalcification of C-S-H gel; x_2 is the calcium ion concentration in pore solution signifying the dissolution of calcium hydroxide, which can be selected as 2 mol/m^3 and 17 mol/m^3 respectively for ordinary Portland cement [68]. It should be noted that calcium leaching would be facilitated due to the continuous consumption of calcium ion from sulfate attack.

However, due to the uncertain chemical compositions of C-S-H gel, the reaction rate constant of calcium leaching under the combined chloride-sulfate attack is still difficult to be determined. As a result, the consumption rate of calcium ions is calculated by the time derivation of solid calcium ion concentration to characterize its kinetics of calcium leaching. The reaction rate of calcium ions induced by leaching effect can be consequently determined by Eq. (17), and the overall reaction rate of calcium ions can be given by the summation of calcium reaction rates caused by ESA in Eq. (7) and leaching in Eq. (17), as shown in Eq. (18).

$$\left(\frac{\partial c_{Ca^{2+}}}{\partial t}\right)_{\text{leaching}} = -\frac{\partial c^{s}_{Ca^{2+}}}{\partial t} \tag{17}$$

$$\frac{\partial c_{Ca^{2+}}}{\partial t} = -\frac{\partial c^{s}_{Ca^{2+}}}{\partial t} - k_1 c_{SO_4^{2-}} c_{Ca^{2+}} \tag{18}$$

2.4. Effect of porosity evolution on concrete diffusivity

As for the expansion mechanisms, it should be noted that arguments still exist between the volume increase theory [42,69] and crystallization pressure theory [70,71] to explain the underlying mechanisms for expansion generation. Compared with the expansion mechanisms, the crystallization pressure mechanisms can explicitly calculate the force required for expansion, which is more explainable in the case of external sulfate attack. However, in order to calculate the crystallization pressure in pore scale, a microscopic model should be established where the pore structures and connectivity must be taken into account. Since the present study mainly focuses on the competitive binding and electrostatic coupling effect rather than concrete volume stability during combined chloride-sulfate attack, and also considering mesoscopic nature of the present model where the pore structures and distributions are not explicitly expressed, the volume increase theory is adopted here.

Assuming that the volume increase is mainly caused by Ettringite formation, the volumetric variations caused by chemical reactions depicted by Eqs. (2)–(4) can be subsequently determined according to literature [42].

$$\frac{\Delta V_i}{V_i} = \frac{M_{\text{AFt}} - M_i - a_i M_{\text{gypsum}}}{M_i + a_i M_{\text{gypsum}}} \quad (i = 1, 2, 3) \tag{19}$$

where M_{AFt}, M_i and M_{gypsum} represent the molar volume of Ettringite, calcium aluminate phases and gypsum respectively (m^3/mol); a_i represents the stoichiometric coefficient of gypsum for chemical reactions in Eqs. (2)–(4). The specific values for volumetric change caused by Ettringite precipitation are given in Table 1. Therefore, the volume variations caused by the Ettringite precipitation in the entire system can be given as

$$\left(\frac{\Delta V}{V}\right)_{\text{AFt}} = \alpha_s C^{\text{AFt}}_{\text{CA}} \quad \text{with} \quad \alpha_s = \sum_{i=1}^{3} \frac{\Delta V_i}{V_i} M_i \lambda_i \tag{20}$$

where $C^{\text{AFt}}_{C_xA} = C_{C_xA,0} - C_{C_xA} - C^{\text{Fs}}_{C_xA}$ is the consumed calcium aluminates to form Ettringite (mol/m^3); $C_{C_xA,0}$ is the initial molar concentration of calcium aluminates; C_{C_xA} is the molar time-variant concentration of calcium aluminates; $C^{\text{Fs}}_{C_xA}$ is the molar concentration of consumed calcium aluminates to form Friedel's salt; α_s represents the summation of volume change per mole of Ettringite precipitation.

Under the combined chloride-sulfate attack, apart from chemical reactions resulting from sulfate ions, chloride ingress can lead to the formation of low-soluble Friedel's salt in Eqs. (10) and (11), which can also take up additional pore space. Similar to Eq. (19), the volume variations caused by Friedel's salt precipitation can be written as

$$\frac{\Delta V_i}{V_i} = \frac{M_{\text{Fs}} - M_i}{M_i} \quad (i = 4, 5) \tag{21}$$

where M_{Fs} represents the molar volume of Friedel's salt. The specific values for volumetric change caused by Friedel's salt formation are also listed in Table 1. It should be noted that the calculated volume change in Eq. (11) gives a negative value. This is because the molar volume of Friedel's salt is less than that of mono-sulfates. However, the summation of volume change in Eqs. (10) and (11), β_s, still yields a positive value, indicating a reduced pore space due to the formation of Friedel's salt. Therefore, the volume change caused by the Friedel's salt precipitation in the system can be given by Eq. (22).

$$\left(\frac{\Delta V}{V}\right)_{\text{Fs}} = \beta_s C^{\text{Fs}}_{\text{CA}} \quad \text{with} \quad \beta_s = \sum_{i=4}^{5} \frac{\Delta V_i}{V_i} M_i \lambda_i \tag{22}$$

In addition to the reduced porosity caused by the precipitation of Ettringite and Friedel's salt, calcium leaching will conversely increase porosity due to the dissolution of calcium hydrate and decalcification of calcium silicate hydrates, which will to some extent release the space occupied by combined sulfate and chloride erosion products. However, due to amorphous and variable stoichiometry characteristics of the C-S-H gel, it is challenging to determine the exact volume variations as a function of continuous decalcification [68]. Consequently, the equivalent molar volume of calcium hydrate, γ_s, is adopted to quantify the volume change due to leaching effect, which can be given as

$$\left(\frac{\Delta V}{V}\right)_{\text{leaching}} = \gamma_s \left(c^{s}_{Ca^{2+},0} - c^{s}_{Ca^{2+}}\right) \tag{23}$$

where $c^{s}_{Ca^{2+},0}$ is the initial content of solid calcium ions before leaching, which can be determined as the summation of the initial content of calcium hydrate, $C_{\text{CH}0}$, and calcium silicate hydrates, $C_{\text{CSH}0}$, as mentioned in Eq. (16). In summary, the total porosity variation under the combined chloride-sulfate attack with the consideration of calcium leaching can be subsequently obtained by Eq. (24). The impact of porosity variation on the ionic diffusivity can also be determined by employing the modified Kozeny-Carman relationship in Eq. (25) [72].

$$\rho = \rho_0 - \left(\frac{\Delta V}{V}\right)_{\text{AFt}} - \left(\frac{\Delta V}{V}\right)_{\text{Fs}} + \left(\frac{\Delta V}{V}\right)_{\text{leaching}} \tag{24}$$

$$H_1(\rho) = \left(\frac{\rho}{\rho_0}\right)^3 \left(\frac{1-\rho_0}{1-\rho}\right)^2 \tag{25}$$

where H_1 is the dimensionless multiplier characterizing the effect of porosity change on concrete diffusivity; ρ represents the porosity; ρ_0 represents the initial capillary porosity which can be determined by the Powers' model [73] as

$$\rho_0 = \frac{w/c - 0.36\alpha}{w/c + 0.32} \tag{26}$$

where w/c signifies water-to-cement ratio; α signifies the maximum hydration degree of ordinary Portland cement paste, and it can be calculated by the Eq. (27) according to literature [74], which was fitted based on a large number of experimental data [75–77].

$$\alpha = 0.239 + 0.745 tanh[3.62(w/c - 0.095)] \tag{27}$$

Table 1
Volumetric variations for chemical reactions caused by sulfate and chloride attack.

Reaction type	i	Chemical reactions	Reactants	$\Delta V_i/V_i$
Sulfate attack	1	Eq. (2)	C_3A	1.25
	2	Eq. (3)	C_4AH_{13}	0.48
	3	Eq. (4)	$C_4A\bar{S}H_{12}$	0.54
Chloride attack	4	Eq. (10)	C_3A	2.05
	5	Eq. (11)	$C_4A\bar{S}H_{12}$	−0.12

2.5. Effect of mechanical damage on concrete diffusivity

The mechanical damage during the combined chloride-sulfate attack is mainly attributed to the formation of expansive products such as gypsum and Ettringite, while Friedel's salt precipitation due to chloride ingress contributes little to the mechanical damage. When expansive volume of gypsum and Ettringite exceeds the free pore space, expansive strain exerted on the pore wall will cause microcracks initiation and propagation, which will further influence the ionic diffusivity. Based on the quantified porosity variations, the expansive volume strain caused by sulfate attack with the influence of calcium leaching being taken into account can be subsequently given by

$$\varepsilon_v = \left(\frac{\Delta V}{V}\right)_{\mathrm{AFt}} - \left(\frac{\Delta V}{V}\right)_{\mathrm{leaching}} - f\rho_0 \tag{28}$$

where ε_v is the expansive volume strain caused by ESA with the consideration of calcium leaching; f is the buffer coefficient characterizing the volume fraction of initial porosity which can offset the expansion of Ettringite without generating stress, and can be empirically taken in the range of 0.05 to 0.4 [59], and a value of 0.23 was selected in this study according to the fitting results mentioned in literature [46]. It should be noted that the buffer coefficient is correlated with the pore size distribution. In other words, the capacity of pores to accommodate the expansions is dependent on the pore size, and small pores with less extra space to accommodate expansions are more likely to firstly generate expansive strains than larger pores [78]. However, considering the mesoscopic model in the present study, the value of f is selected as a fixed value and a more detailed parametric analysis of its potential influences on modelling results will be conduced in Section 4.1. According to studies by Sarkar et al. [79], the influence of mechanical damage on concrete diffusivity can be calculated as

$$H_2(C_d) = \left(1 + \frac{32}{9}C_d\right) + D_p \tag{29}$$

$$C_d = \begin{cases} 0.16(1-\varepsilon_{th}/\varepsilon)^{2.3} & \text{for } \varepsilon > \varepsilon_{th} \\ 0 & \text{for } \varepsilon \le \varepsilon_{th} \end{cases} \tag{30}$$

$$D_p = \begin{cases} 0 & C_d < C_{dc} \\ (C_d - C_{dc})^2/(C_{dec} - C_d) & C_{dc} \le C_d < C_{dec} \end{cases} \tag{31}$$

$$\begin{cases} \dfrac{\partial c_{\mathrm{SO_4^{2-}}}}{\partial t} = div\left(D_{\mathrm{SO_4^{2-}}}\nabla c_{\mathrm{SO_4^{2-}}} + \dfrac{F}{RT}z_{\mathrm{SO_4^{2-}}}D_{\mathrm{SO_4^{2-}}}c_{\mathrm{SO_4^{2-}}}\nabla\varphi\right) - k_1 c_{\mathrm{SO_4^{2-}}}c_{\mathrm{Ca^{2+}}} & k = \mathrm{SO_4^{2-}} \\ \dfrac{\partial c_{\mathrm{Ca^{2+}}}}{\partial t} = div\left(D_{\mathrm{Ca^{2+}}}\nabla c_{\mathrm{Ca^{2+}}} + \dfrac{F}{RT}z_{\mathrm{Ca^{2+}}}D_{\mathrm{Ca^{2+}}}c_{\mathrm{Ca^{2+}}}\nabla\varphi\right) - k_1 c_{\mathrm{SO_4^{2-}}}c_{\mathrm{Ca^{2+}}} - \dfrac{\partial c^s_{\mathrm{Ca^{2+}}}}{\partial t} & k = \mathrm{Ca^{2+}} \\ \dfrac{\partial c_{\mathrm{Cl^-}}}{\partial t} = div\left(D_{\mathrm{Cl^-}}\nabla c_{\mathrm{Cl^-}} + \dfrac{F}{RT}z_{\mathrm{Cl^-}}D_{\mathrm{Cl^-}}c_{\mathrm{Cl^-}}\nabla\varphi\right) - \dfrac{\partial\left(c^{\mathrm{chem}}_{\mathrm{Cl^-}} + c^{\mathrm{phy}}_{\mathrm{Cl^-}}\right)}{\partial t} & k = \mathrm{Cl^-} \\ \dfrac{\partial c_k}{\partial t} = div\left(D_k\nabla c_k + \dfrac{F}{RT}z_k D_k c_k \nabla\varphi\right) & k = \text{others} \end{cases} \tag{36}$$

where H_2 is the multiplier characterizing the influence of mechanical damage on material diffusivity; C_d represents the crack density; C_{dc} and C_{dec} are two percolation thresholds proposed by Sarkar et al. to quantify the conduction percolation and rigidity percolation respectively; ε is the uniaxial strain determined as $\varepsilon_v/3$; ε_{th} is the threshold strain signifying crack initiation; D_p is the diffusivity in the percolation regime. With the consideration of both porosity variation and mechanical damage, the time- and space-dependent ionic diffusivity can be calculated by the initial effective ionic diffusion coefficient in sound concrete, D_k^0, multiplied with H_1 and H_2 as

$$D_k = H_1(\rho)\cdot H_2(C_d)\cdot D_k^0 \tag{32}$$

In this study, the initial effective diffusion coefficients are determined by adopting the following equation

$$D_k^0 = D_k^{free}/\sigma \tag{33}$$

where D_k^{free} is the ionic diffusivity in bulk water; pore structure parameter σ is related to porosity and cement type, which can be calculated according to literature [80].

2.6. Multi-ionic transport

The transport behavior of various ionic species in cementitious materials can be described by the Nernst-Planck equation. In a completely saturated condition, the effect of convection on ionic transport can be ignored. The ionic transport is mainly driven by the concentration gradient and potential gradient as shown in Eq. (34). The time-dependent ionic concentrations can then be derived with the consideration of reaction term caused by chemical reactions, as shown in Eq. (35).

$$J_k = -D_k\nabla c_k - D_k c_k\frac{z_k F}{RT}\nabla\varphi \tag{34}$$

$$\frac{\partial c_k}{\partial t} = -\nabla\cdot J_k + S_k \tag{35}$$

where J_k, D_k and c_k are the ionic flux, diffusion coefficient and molar concentration of k-th ionic species in concrete pore solution; z_k is the charge number carried by k-th ion; F is the Faraday constant (9.6488×10^4C·mol^{-1}); R is the ideal gas constant (8.314 J·mol^{-1}·K^{-1}); T is the absolute temperature which is taken as the room temperature (298 K); φ is the electrostatic potential; S_k is the reaction term reflecting the ionic consumption induced by chemical reactions during the combined chloride-sulfate attack. Substituting chemical reaction terms derived from Section 2.1 to Section 2.3 into Eq. (35), the reactive transport equations for various ionic species can be consequently given by the following equation, and other ionic species (k = others) considered in this model include OH^-, K+ and Na^+.

Note that ionic species in concrete pore solution are not always compliant with the electric neutrality hypothesis, and the coexistence of various ionic species will result in an electrochemical coupling effect. In other words, the ionic charge imbalance and the consequently induced electrostatic potential in concrete pore solution should be taken into account [81]. In this case, the traditional Laplacian equation, $\Delta\varphi = 0$, used to solve electrostatic potential distribution under the electric neutrality assumption should be replaced by the more rigorous Poisson equation based on the constitutive electrochemical law as

$$\Delta\varphi = -\frac{1}{\varepsilon_0\varepsilon_r}\left(F\sum_{k=1}^{n} z_k c_k\right) \tag{37}$$

where ε_0 represents the vacuum dielectric constant (8.854×10^{-12} F·m^{-1}); ε_r represents the relative dielectric constant of water at the temperature of 298 K which is taken as 78.3; $F\sum_{k=1}^{n} z_k c_k$ determines the charge volume density caused by charge imbalance in concrete pore solution (C·m^{-3}).

3. Calibration and validation

In this section, the experimental results reported by Chen et al. [51] was firstly selected for calibration, where the independent parameters of the studied case were quantified following the test and trial method. Subsequently, in the model validation, without changing the calibrated parameters, the modelling results were compared with results from two sets of experiment by Jin et al. [35] and Maes [82] under both single chloride attack and combined chloride-sulfate attack respectively. The total chloride content which can reflect the competitive binding aspect, and the free chloride concentrations which can reflect the ionic transport aspect were selected and compared.

3.1. Calibration against experimental results by Chen et al.

3.1.1. Problem description and model setups for parameter calibration

Chen et al. [51] prepared cubic samples sized 100 mm with ordinary Portland cement (P. O. 42.5 grade according to Chinese Standard GB 175–2007 [83]) and a water cement ratio of 0.45. Natural gravel size ranging from 5 mm to 20 mm with continuous grading was selected as coarse aggregates, and artificial-sand with fineness modulus 2.94 served as the fine aggregates. After reaching the age of 28 day, one surface of the specimens were exposed to the mixed solution of 10 % NaCl and 5.0 % Na_2SO_4 (combined chloride-sulfate attack) for 300 days under room temperature. Chloride and sulfate ions concentrations were measured by analyzing power samples by drilling cores from the exposure surface.

As for the cases of numerical setups, the two-dimensional cross section sized 100 mm × 100 mm with one surface exposed to the external solutions was established, as shown in Fig. 2(a). There are three phases in the model, namely coarse aggregates represented by random polygon, cement matrix, and interfacial transitional zone (ITZ) between cement matrix and coarse aggregates. After converting the fuller grading curve from into 2D distribution, the coarse aggregates were generated according to the size range mentioned by Chen et al., and randomly placed in concrete bulk to meet a volume fraction of 45 %, which was roughly in accordance with the mix proportion in experiment. Moreover, the ITZ were modelled with a thickness of 80 μm. It should be noted that the thickness of ITZ commonly observed in concrete is between 20 μm and 40 μm, and the diffusion coefficients are reported to be 6–12 times larger than these in cement bulk [84,85]. However, in order to avoid poor quality meshing results, the ITZ thickness was enlarged to 80 μm with reduced ionic diffusion coefficients which were taken as 3 times larger than those in cement bulk. Meanwhile, limited by the two-dimensional nature of the presented model, the heterogeneity along the longitudinal direction cannot be accurately reflected, e.g. changing the ITZ percolation properties. However, as mentioned in the experimental program, the specimens were immersed in solutions for a long period of time, so it is reasonable to assume that the concrete was saturated, and the percolation caused by water transport in and out ITZs is less significant. Therefore, the two-dimensional simplification is adopted here as a compromise, but more advanced and realistic three-dimensional models should still be preferred in the future researches.

In addition, the element meshing size of the model should be determined to ensure a convergent and stable numerical solution. Therefore, a mesh refinement study was conducted by refining meshing size until little difference in numerical results can be observed with further refinement. It is also worth noting that for ionic transport process with migration, the element size h should be such that the Peclet number ($h{\cdot}u/D$, where u is the ionic migration velocity, and D denotes ionic diffusion coefficient) is less than 1 to ensure convergence. As a result, the finite discretization scheme with a minimum element size of 1 μm was adopted to ensure a convergent and stable numerical solution, as shown in Fig. 2(b). It should be noted that due to the lower permeability of coarse aggregates compared to cement matrix and ITZ [86], the coarse aggregates were considered as impermeable, and the corresponding regions were therefore not meshed to optimize the computational cost. In the following sections, unless otherwise mentioned, the model establishment would follow the abovementioned procedures by

Table 2
Pre-calculated parameters by the experimental information of Chen et al. [51].

Parameters	Symbols	Value
Solid initial concentrations	$C_{CxA,0}$	106.42 mol/m^3
	C_{CH0}	122.68 mol/m^3
	C_{CSH0}	554.34 mol/m^3
Volume change coefficient	α_s	1.60×10^{-4} m^3/mol
	β_s	0.10×10^{-4} m^3/mol
stoichiometric coefficient	q	2.13
Initial porosity	ρ_0	16.18 %

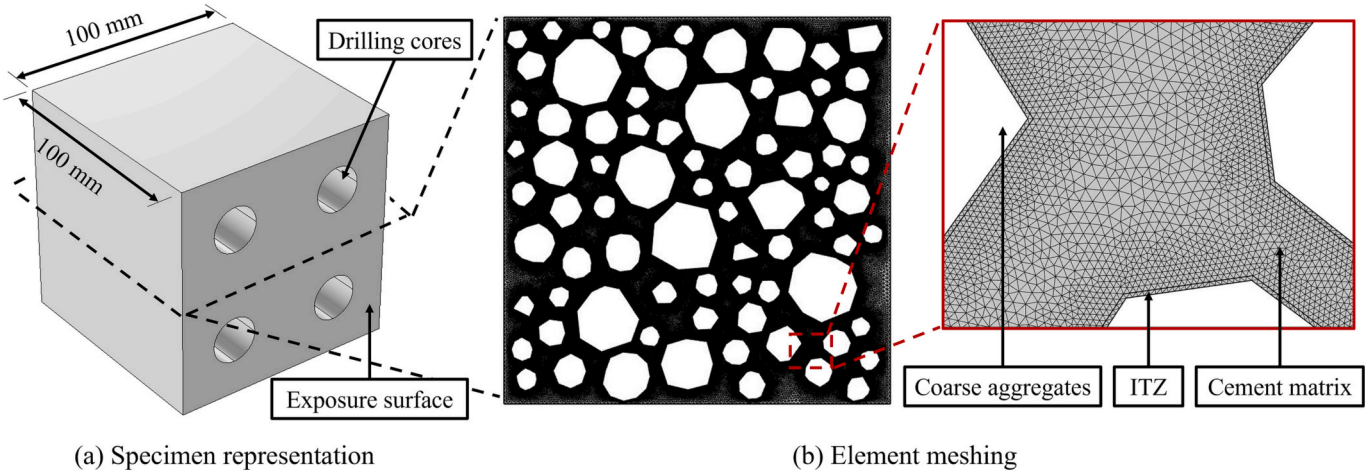


Fig. 2. (a) geometric representation and (b) finite discretization scheme of the numerical model with three different phases: coarse aggregates, ITZ and cement matrix.

Table 3
Calibrated parameters against experimental data by Chen et al.

Parameters	Symbols	Value
Initial effective diffusion coefficients in cement paste	$D^0_{Cl^-}$	4.41×10^{-12} m^2/s
	$D^0_{SO_4^{2-}}$	2.30×10^{-12} m^2/s
	$D^0_{OH^-}$	11.42×10^{-12} m^2/s
	$D^0_{Ca^{2+}}$	1.71×10^{-12} m^2/s
	$D^0_{K^+}$	4.24×10^{-12} m^2/s
	$D^0_{Na^+}$	2.89×10^{-12} m^2/s
Reaction rate constant for Eq. (1)	k_1	3.66×10^{-8} m^3/mol/s
Reaction rate constant for Eq. (5)	k_2	1.22×10^{-9} m^3/mol/s
Reaction constants for chloride binding	K_{chem}	0.551
	K_{phy}	0.070

adjusting the sample size, aggregate volume, and boundary ionic concentrations according to the mixture proportions and exposure conditions provided by different experiments.

3.1.2. Parameter quantification

Before conducting parameter calibration, the initial content of the clinker minerals can be quantified by the Bogue calculation according to the cement chemical compositions and mixture proportions provided by Chen et al. Subsequently, the initial content of calcium aluminates $C_{CxA,0}$ and stoichiometric coefficient q adopted in the numerical model were calculated according to the study by Tixier [59]. The initial content of portlandite and calcium silica hydrates were determined following the method in literature [87]. The boundary concentrations were set according to the experimental exposure solutions by converting the weight percentage to molar concentration. According to the provided experimental information, parameters which can be pre-calculated by the proposed formulae are listed in Table 2.

The parameter calibration process follows a test and trial method. Values calculated by formulae or collected from existing studies will serve as a preliminary value (reference value), and then by adjusting the value to reduce the relative errors with experimental data. The detailed procedure can be described as follows, and the calibrated values were summarized in Table 3.

1) Firstly, the calculated initial effective diffusion coefficients from Eq. (33) were regarded as preliminary values. By comparing with experimentally measured free chloride and sulfate content, the chloride and sulfate diffusion coefficients were calibrated, as shown in Fig. 3(a) and (b). The diffusion coefficients of other ionic species were accordingly adjusted by the same magnitude.
2) Besides, chemical reaction parameters will be calibrated by comparing total chloride and sulfate concentrations. Because the free ionic concentrations have already been calibrated in the previous step, and the reaction parameters will mostly influence the ionic concentrations in bound state. Therefore, chemical reaction parameters can be calibrated by comparing with the total ionic concentrations. Initially, the collected values for sulfate and chloride binding from literatures [46,53] will serve as the preliminary value, and then adjustments were carried out to match the total chloride and sulfate concentrations with experimental measurements, as shown in Fig. 3(c) and (d).

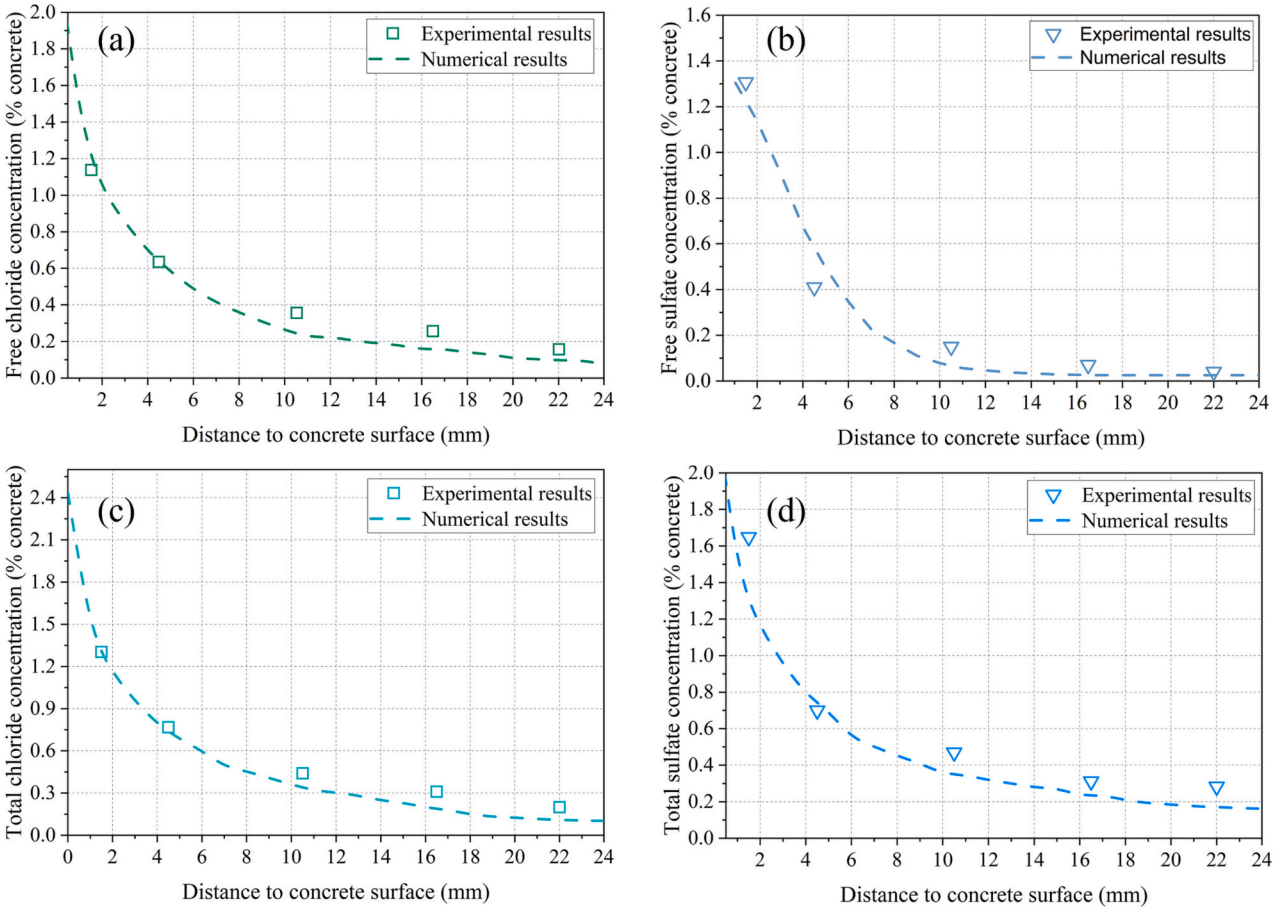


Fig. 3. Parameter calibration by comparing (a) free chloride concentration, (b) total chloride concentration, (c) free sulfate concentration and (d) total sulfate concentration.

Table 4
Pre-calculated parameters by the experimental information of Maes [82].

Parameters	Symbols	Value
Solid initial concentrations	$C_{CxA,0}$	102.80 mol/m^3
	C_{CH0}	410.58 mol/m^3
	C_{CSH0}	612.25 mol/m^3
Volume change coefficient	α_s	1.58×10^{-4} m^3/mol
	β_s	0.08×10^{-4} m^3/mol
stoichiometric coefficient	q	2.13
Initial porosity	ρ_0	16.18 %

3.2. Validation against experimental results by Maes

3.2.1. Problem description and model setups for model validation

The experiment conducted by Maes [82] was firstly selected to proof the validity of the numerical model. Maes tested mortar specimens mixed with ordinary Portland cement and the water to cement ratio was also maintained at 0.45 which was in accordance with the experiment used for parameter calibration. Cylindrical samples with a diameter of 100 mm and a thickness of 50 mm were prepared. At the age of 28 days, the specimens were immersed saturated calcium hydroxide solution for 7 days. Then they were put into the combined NaCl (165 g/l) and Na_2SO_4 (50 g/l) solutions for 28 weeks with only one surface exposed. The total chloride content was then measured by acid-extraction at 14 weeks and 28 weeks respectively. According to the mineralogical compositions and mixture proportions provided in the experiment, the pre-calculated parameters are listed in Table 4. The boundary ionic concentrations were also set according to the adopted exposure solution mentioned in the experiment.

3.2.2. Comparison on total chloride concentration

By inputting the pre-calculated parameters which are dependent on the cement mineralogical compositions, and the calibrated parameters which tend to hold close values for ordinary Portland cement with similar mixture proportions, numerical simulations of the experimental exposure test can be conducted. Comparison of the total chloride contents under both combined chloride-sulfate attack and single chloride attack have been plotted in Fig. 4. It can be found that the numerical results agree well with the experimental data, and the trend of increased total chloride content with the extension of exposure time can be noticed in both cases. In addition, the addition of sulfate in exposed solution would reduce the total chloride content, suggesting a competitive antagonism between chloride and sulfate ions.

3.3. Validation against experimental results by Jin et al.

3.3.1. Problem description and model setups for model validation

The experiment by Jin et al. [35] was also selected to further validate the proposed numerical model. In the experimental procedure, concrete prism specimens with the dimension of 40 mm × 40 mm × 160 mm were prepared with ordinary Portland cement P. O. 42.5 at a water to cement ratio of 0.45, where the cement type and *w/c* ratio were the same with the experiment cited for calibration. River sand with a fineness modulus of 2.6 was adopted as the fine aggregates, and crushed limestone with maximum size of 10 mm were selected as coarse aggregates. After curing for 60 days, specimens were immersed in 3.5 % NaCl solution and composite solution of 3.5 % NaCl and 5.0 % Na_2SO_4 for 800 days under room temperature. Free chloride concentration in concrete were measured by drilling cores at 5 mm intervals. Apparent chloride diffusion coefficients in both NaCl solution and composited solution were also fitted according to the tested results.

Similarly, according to the cement chemical compositions and concrete mix proportions in experiment conducted by Jin et al., parameters such as the initial content of calcium aluminate phases, portlandite and calcium silica hydrates, as well as the stoichiometric coefficient can be pre-calculated, as provided by Table 5. The boundary concentrations were set according to the experimental exposure solution (i.e., 3.5 % NaCl solution and 3.5 % NaCl +5 % Na_2SO_4 composite solution respectively). The calibrated ionic diffusivities and reaction kinetics parameters in Section 3.2.2 were kept as the same in this section to proof the validity of the proposed model.

3.3.2. Comparison on free chloride concentration

Fig. 5 compares free chloride concentrations in concrete exposed to sodium chloride solution and composite solution of sodium chloride and sodium sulfate. It can be observed that the numerical results agree well with the experiment ones. Chloride concentration gradually reduces along with concrete cover depth, and increases with the extension of exposure duration. The existence of sulfate can hinder chloride penetration and lead to a smaller free chloride concentration in concrete. This suggests that the sulfate ions can improve the concrete's chloride resistance due to the coupling between chloride and sulfate ions chemical reactions (i.e. combined chloride-sulfate attack), and this feature can be well captured by the numerical model. Moreover, it is shown that the most obvious increase in chloride content is from 90 days to 250 days, while the increase after 250 days is less obvious. This is because the formation of expansive products reduces porosity and blocks subsequent chloride penetrations.

3.3.3. Comparison on apparent chloride diffusion coefficient

The apparent chloride diffusion coefficients fitted from experimental and numerical data based on Fick's law are compared in Fig. 6 at different exposure durations, where the error bar shows potential value range with 95 % confidence bounds. It can be seen that the apparent diffusion coefficients gradually decrease over time, and the numerical results are basically consistent with the experimental data. Besides, the apparent diffusion coefficients fitted from composited solution are generally smaller than those from pure sodium chloride solution, which

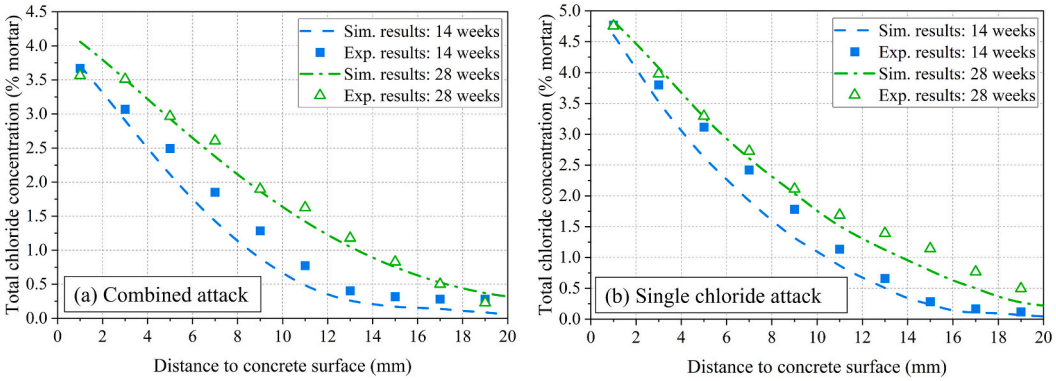


Fig. 4. Total chloride concentrations under (a) combined chloride-sulfate attack and (b) single chloride attack compared against experiment results from Maes.

Table 5
Pre-calculated parameters by the experimental information of Jin et al. [35].

Parameters	Symbols	Value
Solid initial concentrations	$C_{CxA,0}$	86.07 mol/m^3
	C_{CH0}	429.07 mol/m^3
	C_{CSH0}	696.84 mol/m^3
Volume change coefficient	α_s	1.67×10^{-4} m^3/mol
	β_s	0.37×10^{-4} m^3/mol
stoichiometric coefficient	q	2.00
Initial porosity	ρ_0	16.18 %

verifies the fact the ingress of sulfate ions can improve concrete chloride resistance by decreasing initial porosity due to gypsum and Ettringite precipitation. Additionally, it can be observed from the error bar that the discreteness of the fitted diffusion coefficients gradually reduces over time. The fitting effect based on numerical results is generally better than that based on experimental results, except for the fitting result of composite solution on the 90th day. This is mainly attributed to the fact that a numerical model can provide more data at different depths and exposure time, which subsequently lead to a better and more robust fitting result.

4. Results and discussion

In this section, a parametric analysis on different values of the buffer coefficient "*f*" on modelling results will firstly be conducted, which aims to provide a more intuitive inspection of its effect on ionic transport and chemical reactions. Subsequently, an overview of modelling results is displayed and discussed here to discern the influence of combined chloride-sulfate attack on ionic concentration, porosity variation and cement chemical composition. Unless otherwise mentioned, the two-dimensional model with a size of 40 mm × 40 mm is exposed to 3.5 % NaCl +5 % Na_2SO_4 composite solution and 3.5 % NaCl solution for 400 days, which is identical to the experimental condition of Jin et al..

4.1. Buffer coefficient "*f*"

In this study, the buffer coefficient characterizing the capacity of accommodating expansions without generating stress (as illustrated in Eq. (28)) was assumed as 0.23 according to the fitting result in literature [46]. However, according to the study by Ikumi et al. [69,88], the value of the buffer capacity would control the initial stage of external sulfate attack. Therefore, it is necessary to analyze the influence of buffer coefficient values on the modelling results, and a parametric analysis regarding the values of the buffer coefficient "*f*" ranging from 0.05 to 0.4 [59] was conducted.

Three evaluation indices: 5 % reaction front of calcium aluminate phases (defined as the depth where 5 % of the calcium aluminates have been consumed), as well as the chloride and sulfate ions penetration depths after 400 day exposure to the composite solution were selected and shown in Fig. 7. It can be found that the front depth is lower when the buffer coefficient increases with more space to accommodate expansions, but the difference in front depth is almost negligible when "*f*" is larger than 0.2, as shown in Fig. 7(a). This is because the accommodating capacity is larger than the maximum volume expansion when the calcium aluminates were completely consumed. Further increase in the

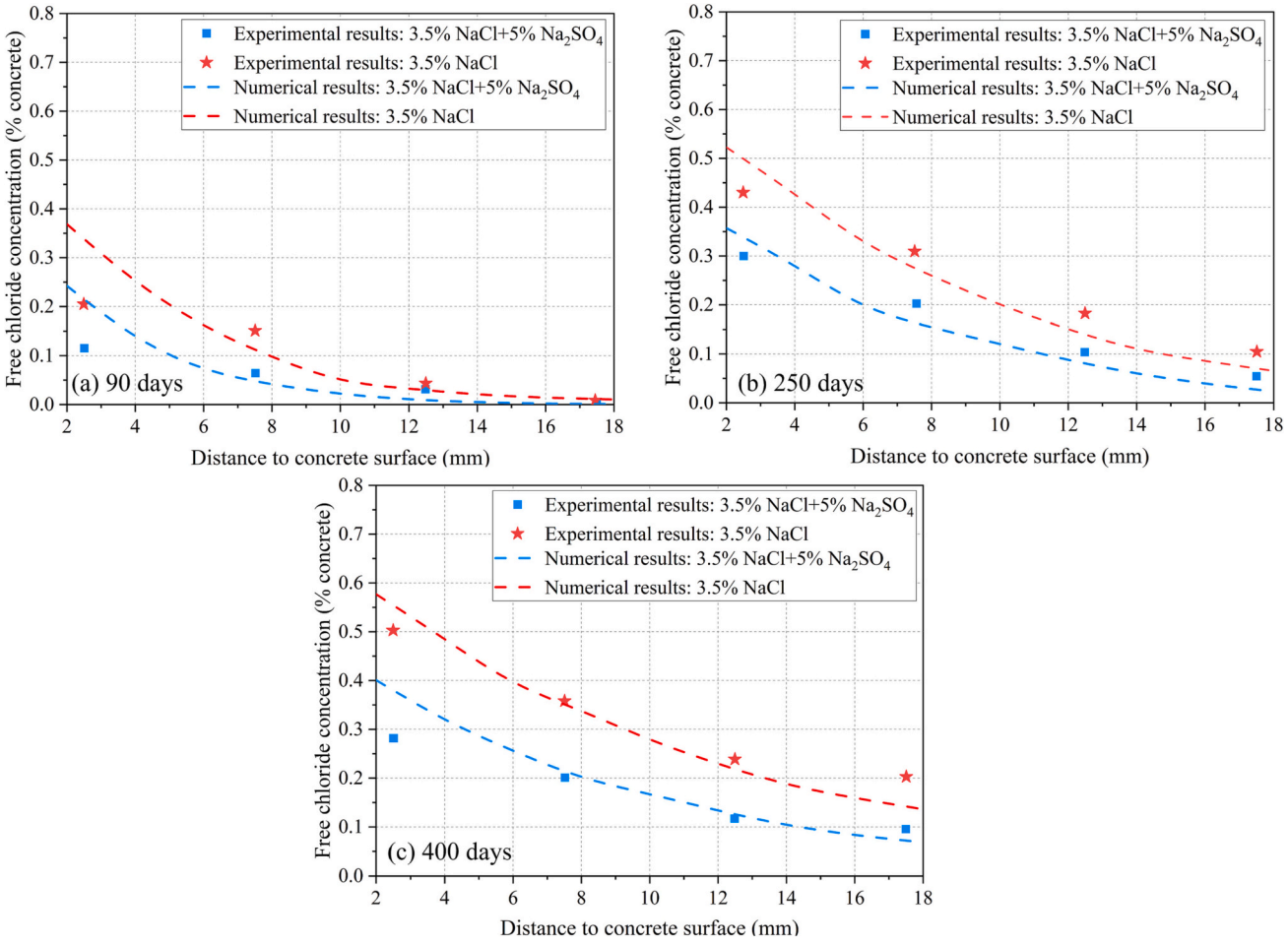


Fig. 5. Comparisons between numerical and experiment results for free chloride concentration after: (a) 90-day, (b) 250-day, and (c) 400-day exposure to different external solutions.

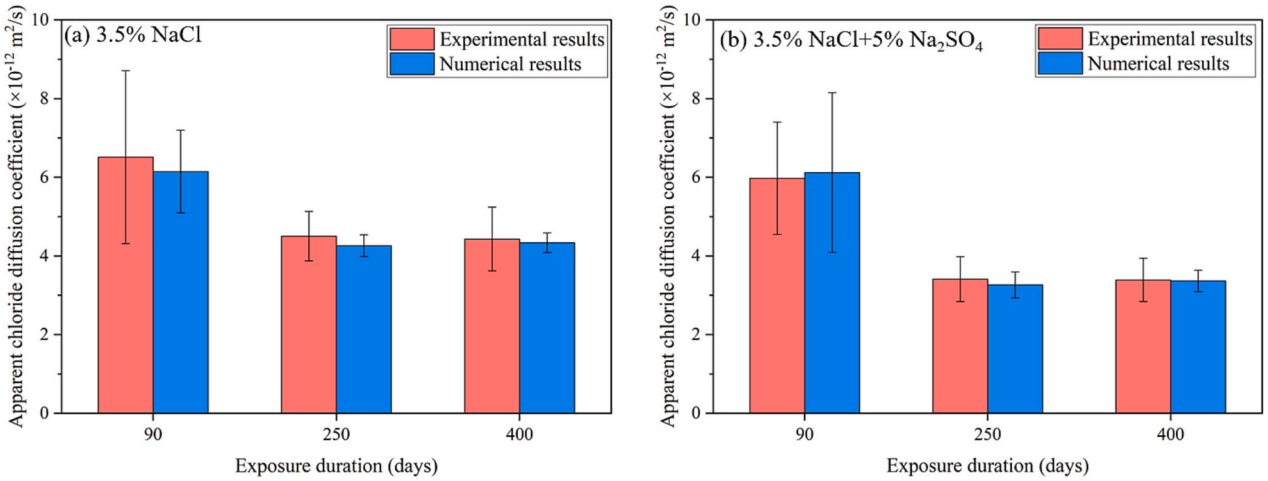


Fig. 6. Comparisons between apparent diffusion coefficients fitted from numerical and experiment data under (a) 3.5 % NaCl solution and (b) 3.5 % NaCl +5 % Na_2SO_4 solution.

buffer coefficient cannot further influence the chemical reaction and ionic transport processes. In other words, even if all of the calcium aluminates have been depleted, the pore structure still extra capacity to accommodate expansions. On the other hand, if the cementitious system has a higher initial calcium aluminates concentration, as illustrated in Fig. 7(b), the front depth for calcium aluminates, chloride and sulfate ions keep decreasing by enlarging the buffer coefficient. As a result, it can be inferred that the influence of buffer coefficient would depend on the calcium aluminates content. For sulfate resisting Portland cement with very few calcium aluminate phases, the influence of buffer coefficient would be less sensitive compared to the ordinary Portland cement.

The influence of buffer coefficient on solid phase compositions were also shown in Fig. 8. With the increase of buffer coefficient, the amount of generated expansive products such as Ettringite gradually reduces. This is because when a certain pore space has more volume to accommodate expansion products without causing cracks, the subsequent transport of sulfate ions will be blocked, which lead to reduced formation of expansive products. On the contrary, if the pore structure has limited space to arrange the expansion, the induced cracks and damage would facilitate the penetration of sulfate ions, which eventually lead to increased amount of expansive products. Similar to the front depth, the influence of buffer coefficient on chemical compositions is more obvious for cases with higher initial calcium aluminates concentrations. In the subsequent section, the buffer coefficient will be fixed at 0.23 according to the fitting results in literature [46] when discussing other aspects of the modelling results.

4.2. Ionic concentration distribution

Because of the competitive adsorption between chloride and sulfate ions, the chloride binding capacity will get influenced due to the coexistence of sulfate ions, which would subsequently affect the ionic profiles. Fig. 9 compares the bound chloride concentration profiles after 400-day chloride attack and combined chloride-sulfate attack. Different to the chloride binding in single chloride ingress, the bound chloride concentration under combined attack is lower before 10 mm depth. This is because the Friedel's salt is depleted due to the ingress of sulfate ions, and the concrete binding capacity is subsequently reduced due to the consumption of mono-sulfates to form Ettringite. In addition, it can be found that bound chloride concentration reached the maximum value at around 17.5 mm depth in case of the combined attack, which is far deeper than that for the pure chloride attack. This is because, on the one hand, the released chloride ions due to sulfate ingress will continuously diffuse into deeper depth under the action of concentration gradient; on the other hand, the calcium aluminates in deeper depth have not yet reacted with sulfate ions to form Ettringite due to the smaller diffusion coefficients of sulfate, so the released chloride ions will firstly reach deeper depth to form Friedel's salt.

In addition to chloride ions, calcium ions which are related to the stability of cement hydration products, as well as the hydroxyl ion which is index of pH value of concrete pore solution should be focused. Fig. 10 shows the molar concentrations of calcium and hydroxyl ions after 400-

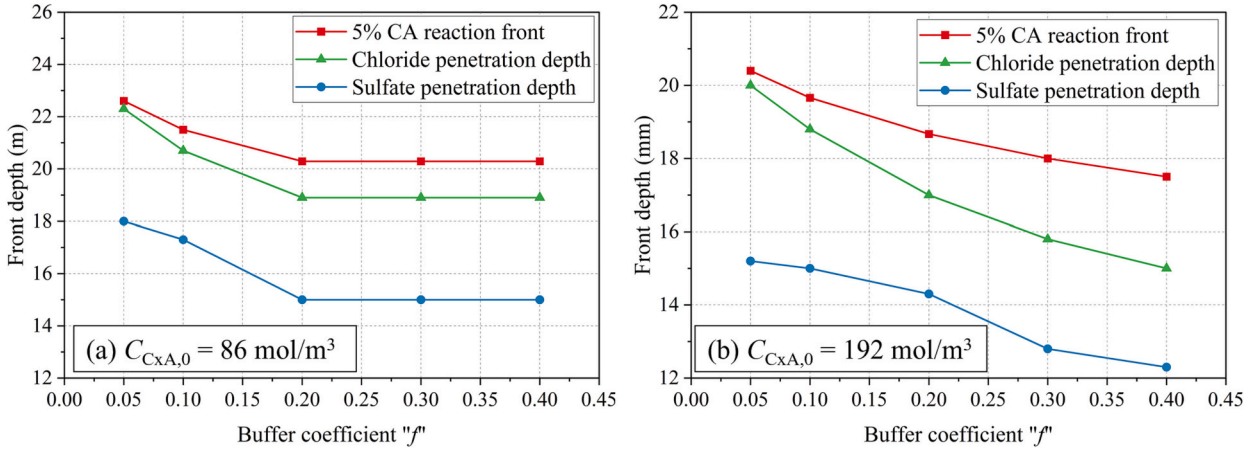


Fig. 7. The influence of buffer coefficient on front depth for concrete with different calcium aluminate concentrations: (a) 86 mol/m^3 and (b) 192 mol/m^3.

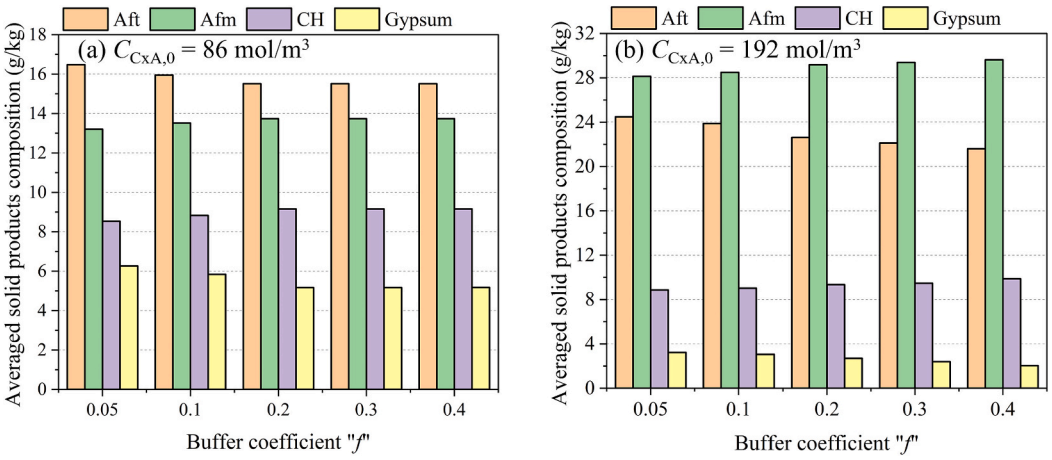


Fig. 8. The influence of buffer coefficient on phase compositions for concrete with different calcium aluminate concentrations: (a) 86 mol/m^3 and (b) 192 mol/m^3.

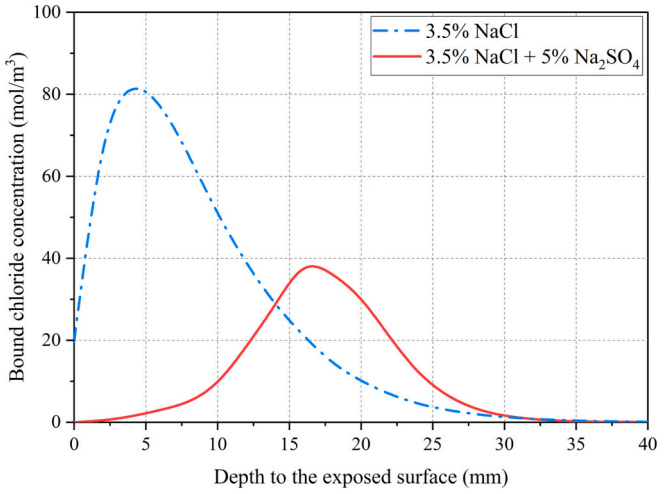


Fig. 9. Bound chloride content under different external solutions after 400-day exposure.

day exposure to 3.5 % NaCl solution (i.e., single chloride attack) and 3.5 % NaCl +5 % Na_2SO_4 composite solution (combined attack), respectively. Compared to the chloride attack, concrete under the combined chloride-sulfate erosion suffers from a more severe calcium leaching effect. Particularly for concrete cover near the exposed surface, the free calcium ion concentrations are close to zero in case of the composite solution. This can be attributed to chemical reactions between calcium and sulfate ions to form secondary gypsum, which will lead to a reduced calcium concentration and facilitate leaching of calcium from cementitious matrix. In addition, the hydroxyl ion concentrations for chloride attack alone and combined attack are similar to each other. However, it can be observed that the hydroxyl ion concentration decreases from the concrete interior to exposed surface, suggesting the alkalinity is reducing with a corrosion risk if embedded with steel reinforcements.

4.3. Chemical composition

The solid product mass percentages relative to concrete are shown in Fig. 11(a) for chloride attack and Fig. 11(b) for combined chloride-sulfate attack respectively. As for pure chloride ingress, it can be seen that monosulfate content close to the exposed surface barely changes, indicating that less chloride ions have reacted with it to form Friedel's salt. This is mainly caused by the depletion of calcium ions due to leaching, which results in a reduced binding capacity in the vicinity of exposure surface. With the increase of concrete depth, however, monosulfate will be gradually consumed to form Friedel's salt. This explanation can be verified by the bound chloride concentration as shown in Fig. 9, where the bound chloride concentration close to exterior surface is relatively lower and then increases to reach the maximum value at a depth where monosulfate content reaches the minimum. As for combined attack, it is shown that gypsum and Ettringite are the main solid precipitation products and mono-sulfates at the vicinity of exposed surface are depleted due to the external sulfate ingress. Additionally, the leaching front under pure chloride attack (approximately 10 mm away from the exposed surface) is smaller than that under combined attack (approximately 17.5 mm away from the exposed surface), which suggests that the sulfate ions can aggravate the intensity of calcium leaching.

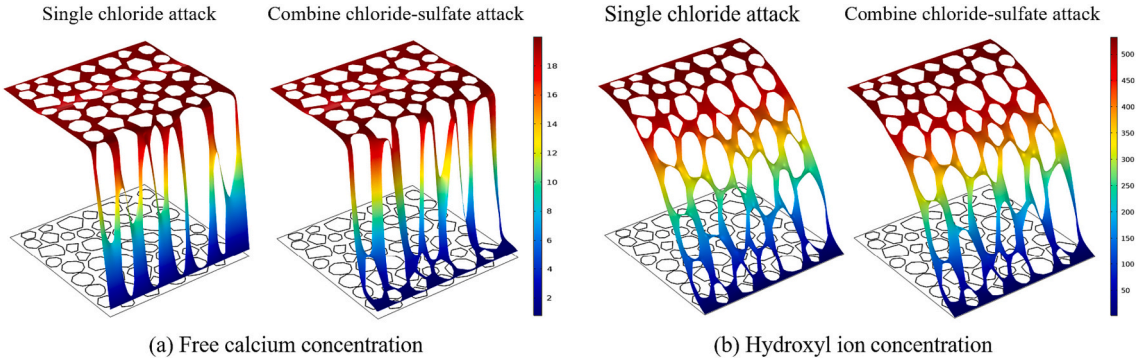


Fig. 10. Calcium and hydroxy ions molar concentrations under different external solutions after 400-day exposure.

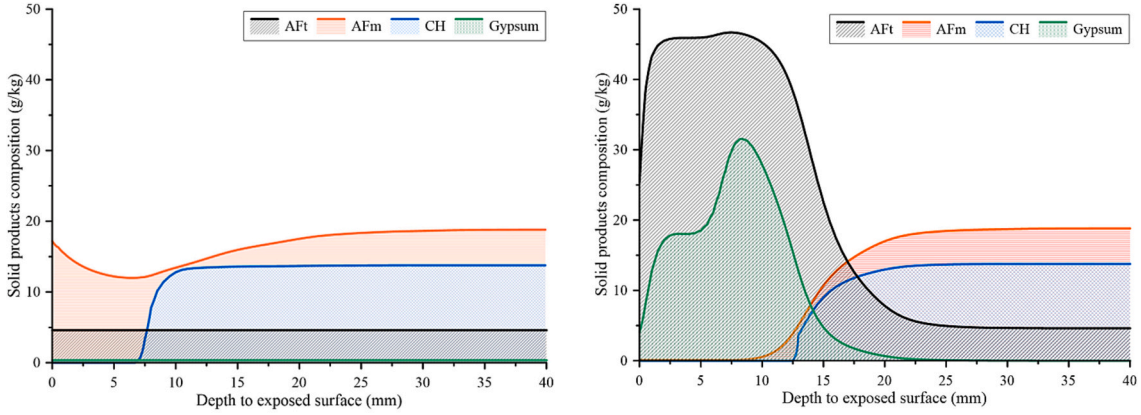


Fig. 11. Concrete solid products content after 400-day exposure under different external solutions: (a) 3.5 % NaCl and (b) 3.5 % NaCl +5 % Na_2SO_4.

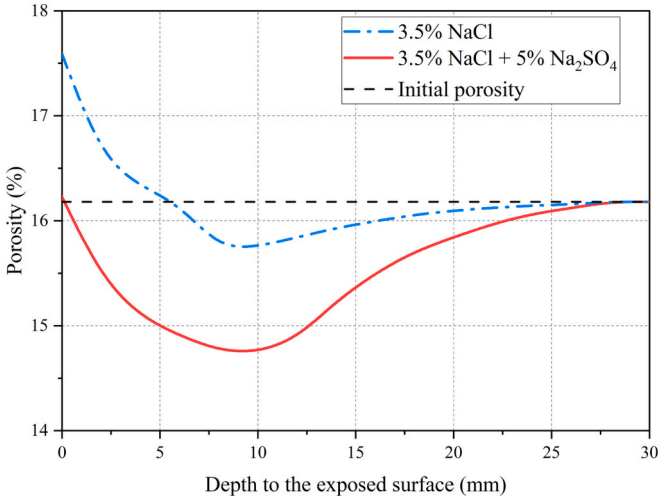


Fig. 12. Porosity variations under different external solutions after 400-day exposure.

4.4. Porosity variation

The porosity variations in 3.5 % NaCl solution and 3.5 % NaCl +5 % Na_2SO_4 composite solution are shown versus concrete cover depth in Fig. 12. A general comparison shows that the concrete porosity under combined attack is lower than that under pure chloride attack. As for concrete cover near to the exposed surface, because of the CH dissolution and C-S-H decalcification caused by calcium leaching, a larger porosity than the initial porosity is witnessed in chloride attack alone. As for concrete exposed to combined solution, the porosity continuously reduces below the initial value within 10 mm cover depth, suggesting that the pore space occupied by solid products precipitation such as Ettringite and gypsum has overwhelmed the void space freed by calcium leaching. The reduced porosity also coincides with solid products distributions displayed in Fig. 11 where the precipitated Ettringite and gypsum products mainly concentrate within the 10 mm depth during the 400-day erosion. In addition, it can be also observed that the minimum porosity for combined attack is lower than that for pure chloride attack, which can be attributed to the larger volume expansion of Ettringite and gypsum compared to that of Friedel's salt. As for cover depth deeper than 30 mm, the porosity barely changes due to the limited diffusion depth of sulfate ions. It should be noted that another reason that the porosity never increases above the initial value is that the damage induced by external sulfate attack was not directly reflected by the porosity variation but by increasing the ionic diffusion coefficients, as shown by Eqs. (24) and (29).

5. Coupling mechanisms investigation

As mentioned previously, there exist both chemical and electrochemical coupling processes during the combined chloride-sulfate attack in cementitious materials. The first one is the coupling among various solid-liquid chemical reactions, and the second one is the electrostatic coupling effect among various ionic species. Therefore, in this section, the competitive chloride-sulfate binding mechanisms are analyzed based on the coupled solid-liquid chemical reactions. Influence factors such as calcium aluminates content, water to cement ratio, and external sulfate ion concentration are systematically changed to investigate their impact on the competitive intensity. After a detailed discussion on the competitive chloride-sulfate binding, the multi-ions coupling will be further considered to further analyze the influence of the electrostatic potential on ionic concentration, transport behavior, and the competitive chloride-sulfate binding intensity.

5.1. Competitive chloride-sulfate binding mechanisms analysis

During the combined chloride-sulfate attack, sulfate and chloride ions will competitively react with calcium aluminates, which will result in distinct features in both free and bound chloride concentrations compared to the single chloride attack. In this section, influencing factors of the coupling interaction, including the calcium aluminates content, the water to cement ratio and the external sulfate concentration, are investigated by comparing both free and bound chloride concentrations along the diffusion depth. Moreover, the net chloride concentration ΔCl^-, which is defined as the difference of chloride concentration under single chloride attack and combined chloride-sulfate attack, is also displayed and compared in order to discuss the competitive mechanisms.

5.1.1. Influence of calcium aluminate content

According to the cement chemical composition information provided in literature [33], three different amounts of tricalcium aluminate (C_3A) ranging from 3.64 % (sulfate resisting type) to 9.65 % are selected to compare both the free and bound chloride concentrations under combined chloride-sulfate attack and single chloride attack situations. The free chloride concentrations and net free chloride concentrations are shown in Fig. 13(a) and (b) respectively. As can be seen from Fig. 13(a), the variation of C_3A content has limited impact on the chloride concentration when only exposed to NaCl solution. As for the combined attack case, however, with the increasing content of C_3A, the free chloride concentration gradually reduces. On the one hand, this is

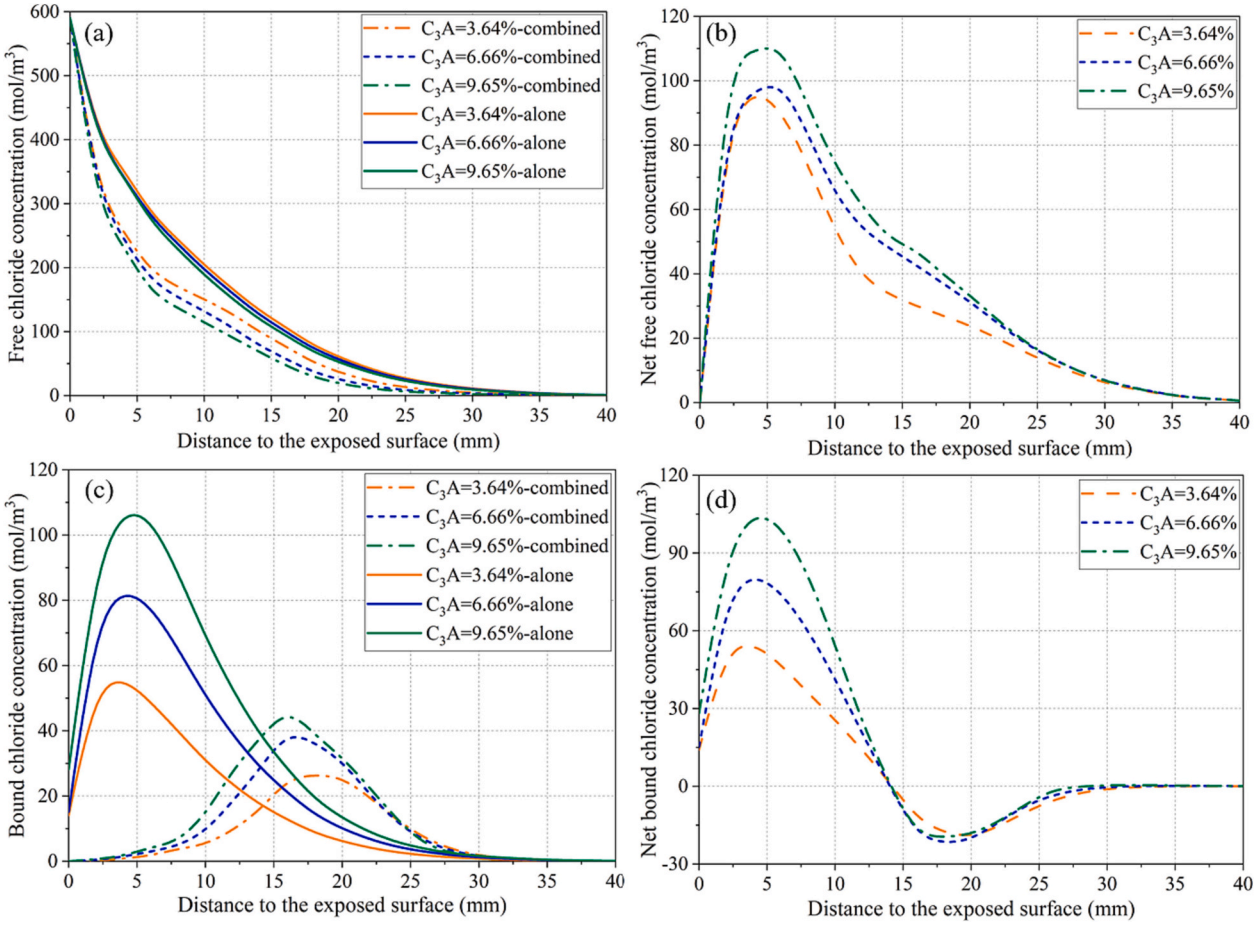


Fig. 13. Influence of calcium aluminates content on (a) free chloride concentration; (b) net free chloride concentration; (c) bound chloride concentration; (d) net bound chloride concentration at various concrete depths.

because with the increase of calcium aluminates content, more expansive products will be precipitated and subsequently densify concrete pore structure, which will hinder the chloride transport process. On the other hand, calcium aluminates phase can also react with chloride to form Friedel's salt, which also leads to a reduced free chloride concentration in cement with high C_3A content. Moreover, it can be seen from Fig. 13(b) that the most significant difference in free chloride concentration occurs at a concrete depth of 5 mm, and the net free chloride concentration (i.e., difference between the solid line and dash line in Fig. 13(a)) increases with the increase of C_3A content, which suggests that higher calcium aluminates content will lead to a more significant competitive mechanism between chloride and sulfate ions.

Fig. 13(c) and (d) display the bound chloride and net bound chloride concentrations in cements with different C_3A contents. It can be observed from Fig. 13(c) that for combined exposure condition, the bound chloride is mostly concentrated in depths ranging from 15 mm to 20 mm, which is deeper than the case of single chloride erosion. This is because due to the lower solubility of Ettringite compared to Friedel's salt and lower diffusion coefficient of sulfate ions, the penetrated sulfate ions can release the previously bound chloride ions into liquid solution, which leads to a reduced chloride binding capacity. This phenomenon is also in line with the findings from an experimental program [51]. The released chloride ions will then diffuse inward to the deeper concrete depth and form Friedel's salt. This feature is well supported by the negative and positive peaks of the net bound chloride concentration between single and combined attack, as shown in Fig. 13(d). The positive peak represents the reduced chloride binding capacity due to the ingress of sulfate ions, and the negative peak is caused by the re-bound chloride ions in deeper concrete cover depth, which have been released from the previously decomposed Friedel's salt due to sulfate ions ingress.

5.1.2. *Influence of water to cement ratio*

Fig. 14(a) illustrates the free chloride concentrations in concrete with different water-to-cement ratios (w/c) under both combined and single chloride attack. In addition to the observation that the existence of sulfate ions will inhibit the chloride diffusion, it can also be seen that for both combined attack and single chloride attack, the increase in water-to-cement ratio results in a higher chloride concentration due to the enlarged porosity. As for net free chloride concentrations, which are displayed in Fig. 14(b), larger water-to-cement ratio leads to a more significant competitive binding relationship between chloride and sulfate ions. The main reason is that the larger water-to-cement ratio will yield a higher porosity, which stimulates the ingress of sulfate ions into concrete and competition with chloride ions to react with hydrated cement phases. Besides, it can also be found that larger water-to-cement ratio leads to the maximum value of net free chloride concentration appearing at the deeper depth of concrete, which is also attributed to the increased ionic diffusivity due to larger water-to-cement ratio.

The bound chloride concentrations with different water-to-cement ratios are given by Fig. 14(c) for concrete exposed to both composite solution and sodium chloride solution alone. It is can be observed that the increase in water-to-cement ratio not only contributes to higher content but also a deeper distribution of bound chloride ions, which is mainly attributed to the loose microstructure and the resultant improved diffusivity caused by larger water-to-cement ratio. Moreover, as for the combined attack, the released chloride ions will continuously diffuse far beyond the diffusion front of sulfate ions to form Friedel's

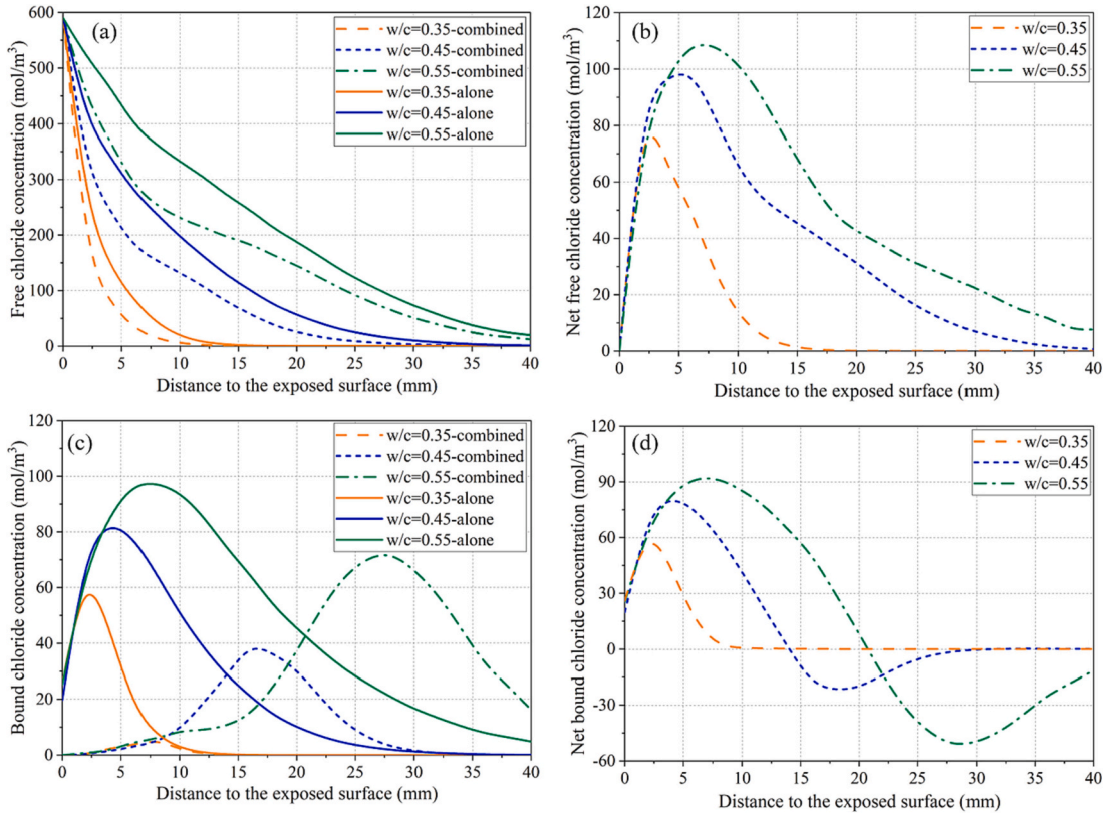


Fig. 14. Influence of water to cement ratio on (a) free chloride concentration; (b) net free chloride concentration; (c) bound chloride concentration; (d) net bound chloride concentration at various concrete depths.

salt. As for the net bound chloride concentration shown in Fig. 14(d), it can be found that, however, no negative peak has been observed when a cement-to-water ratio of 0.35 is adopted. This is because, on the one hand, the reduced porosity hinders the penetration process of chloride, which in turn reduces the content of bound chloride ions. On the other hand, due to the presence of sulfate ions, expansive products will be formed to further densify concrete pore structure and block the existing transport pathways. Therefore, the competitive mechanism has limited impact on concrete depth deeper than 15 mm when the water-to-cement ratio is selected as 0.35.

5.1.3. Influence of sulfate ion concentration

The free chloride concentrations for concrete exposed to external solutions with various sulfate ions strength are shown in Fig. 15(a). It can be seen that, despite the small variation, higher sulfate concentration results in a lower free chloride concentration due to the formation of expansive products and filling voids in cement matrix. In Fig. 15(b) where the net free chloride concentration is shown, the increase in sulfate ion strength results in a larger free chloride concentration difference between combined attack and single chloride attack, which manifests a more significant competitive mechanism. However, the difference contributed by higher sulfate ions becomes less obvious when the cover depth is larger than 20 mm. This is mainly because the formation of expansive products such as Ettringite and gypsum will block the subsequent transport of sulfate ions from external solutions. Therefore, it can be inferred that higher sulfate ion concentration only has a limited impact range along cover depth on the competitive mechanism.

The bound chloride concentrations in concrete exposed to different solutions are shown in Fig. 15(c). As expected, higher sulfate ion concentration leads to a reduced binding capacity of cement matrix. It should be noted that although more chloride can be released into pore solution under a higher sulfate ion concentration, due to the formation of expansive products and pore-filling effect, only part of the released chloride can diffuse inward and get re-bound. This explains the fact that only a smaller amount of bound chloride ions is witnessed for concrete exposed to a mixed solution with highly concentrated sulfate ions. In addition, Fig. 15(d) illustrates the net bound chloride concentration when exposed to mixed solutions with various sulfate ion concentrations. It is found that the mixed solution with 2 % sulfates leads to the most negative peak value. This feature is consistent with the bound chloride concentration displayed in Fig. 15(c) in which concrete exposed to 2 % Na_2SO_4 + 3.5 % NaCl solution possesses the highest content of bound chloride content compared to the other two mixed solutions. The main reason includes the following two aspects. Firstly, because of the competitive mechanism, penetrated sulfate ions can break chemical equilibrium between bound and free chloride, which will release chloride ions into concrete pore solution. Secondly, because the sulfate ion content is relatively smaller, the pore-filling effect caused by sulfate-bearing expansive products is not that obvious. Therefore, the released chloride ions can still diffuse inward to form Friedel's salt.

5.2. Inherent combined coupling mechanisms analysis

5.2.1. Electrostatic potential caused by multi-ions coupling

It should be noted that the ionic charge in concrete pore solution does not always meet the condition of electric neutrality, and the inherent charge imbalance will induce an electrostatic potential inside concrete which in turn affects the ionic transport behavior. In this study, the electrostatic potential distribution is depicted by the Poisson equation based on the constitutive electrochemical law, as shown in Eq. (37), and the corresponding distribution at various time is shown in Fig. 16 as a function of concrete cover depth. It can be seen that a positive electrostatic potential is generated inside concrete pore solution, and the amplitude gradually increases over time. In addition, with the extension of erosion time, the deeper position of the concrete cover will gradually deviate from the electric neutral state and produce a positive electric

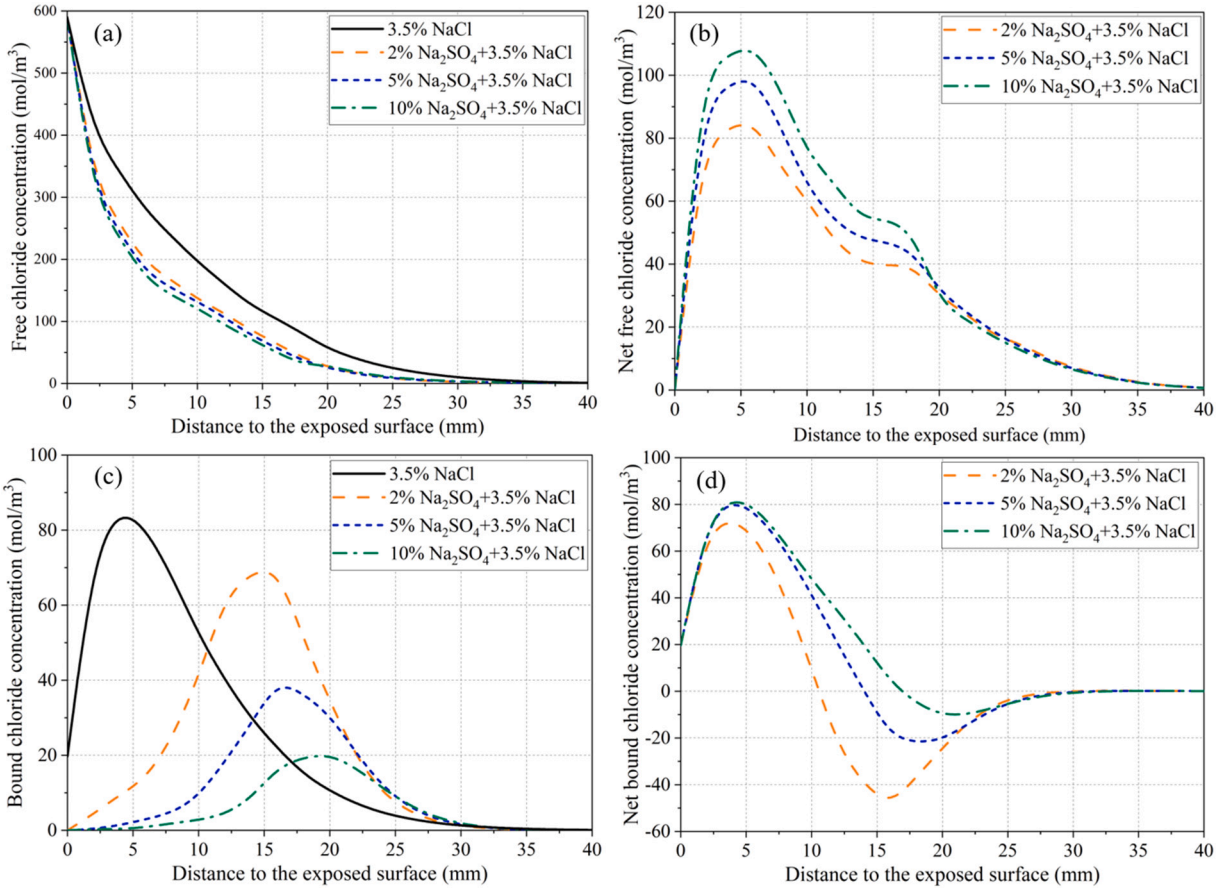


Fig. 15. Influence of sulfate concentration on (a) free chloride concentration; (b) net free chloride concentration; (c) bound chloride concentration; (d) net bound chloride concentration at various concrete depths.

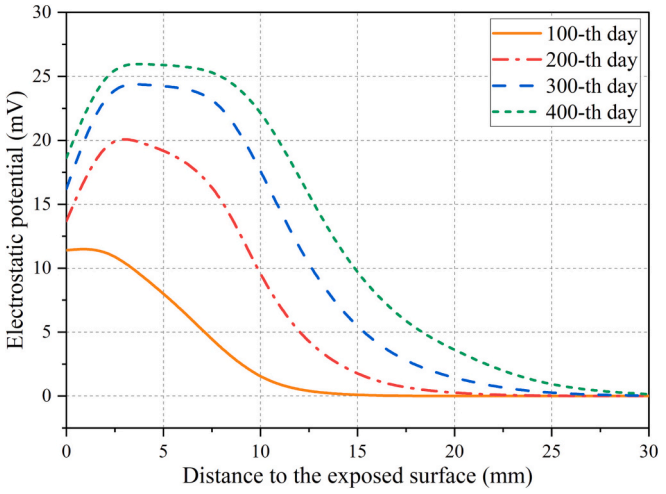


Fig. 16. Distribution of electrostatic potential along concrete cover depth at various time.

field because of the inherent charge imbalance. This can be explained by the fact that the ingress of external aggressive ions such as chloride and sulfates, as well as leaching of calcium ions break the previous equilibrium condition. Therefore, it can be concluded that the external combined chloride-sulfate attack will lead to a non-negligible electrostatic potential in concrete pore solution system. For long-term durability issues involved with ionic penetration, this potential caused by the electrochemical coupling effect would fundamentally affect the ionic transport and further change the deterioration process [81,89], which will be elaborated in the following sections.

5.2.2. *Chloride and sulfate content under electrochemical coupling effect*

The comparison of time and spatial distribution of free chloride concentrations with and without the consideration of electrochemical multi-ions coupling effect is given in Fig. 17. It shows that neglecting multi-ions coupling effect will lead to an underestimated chloride concentration, and this effect will be amplified with the increase in both exposure time and concrete cover depth. This is because apart from the concentration gradient, the positive electrostatic potential caused by ionic charge imbalance will also contribute to the penetration of negative ions such as chloride. A closer observation also finds that the most significant difference occurs between 5 mm and 15 mm of concrete cover. After a 400-day exposure, as shown in Fig. 17(d), ignoring the interaction among various ionic species will result in a 1.25 times lower chloride concentration, and most differences are located within 20 mm concrete cover thickness, which is commonly the thickness of concrete protective cover layer of steel reinforcement. Consequently, it can be indicated that the electric neutrality hypothesis will lead to an underestimated chloride content at the steel reinforcement surface, and the resultant overestimation of corrosion initiation time is also non-conservative.

In addition to chloride, the comparison of free sulfate ion concentrations for cases with and without considering the multi-ions coupling effect is displayed in Fig. 18. Similar to chloride ion, neglecting multi-ions coupling will lead to a smaller predictive result of sulfate concentration. Moreover, compared to the case which takes the multi-ions coupling effect into account, the electric neutrality hypothesis also results in a smaller penetration depth of sulfate ion. However, some

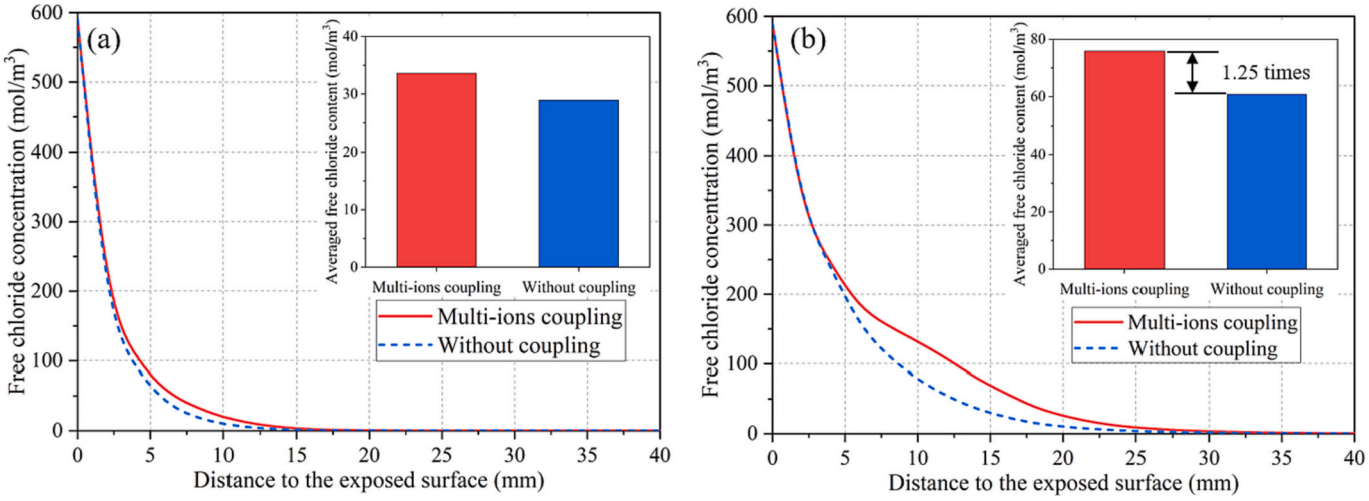


Fig. 17. Comparison of free chloride concentrations for cases with and without multi-ions coupling effect at different time intervals: (a) 100-th day and (b) 400-th day.

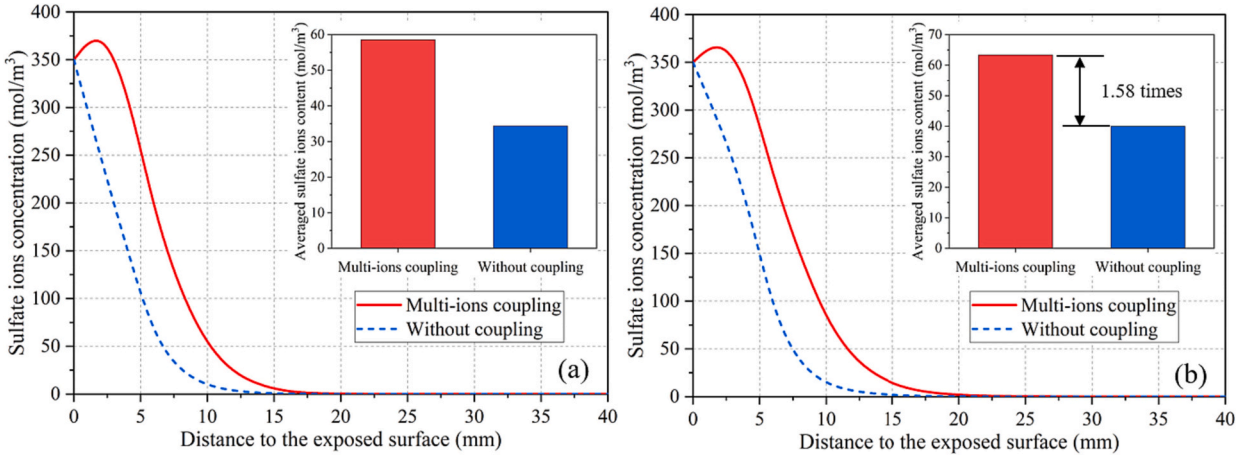


Fig. 18. Comparison of free sulfate concentrations for cases with and without multi-ions coupling effect at different time intervals: (a) 100-th day and (b) 400-th.

different features compared to the chloride concentration distribution can also be found. On the one hand, it can be seen that in terms of sulfate ions, the concentration differences caused by electrochemical coupling effect are even more significant than those of chloride ions, in which the sulfate ions concentrations can reach 1.58 times higher than cases with electroneutrality assumption. On the other hand, because of the ionic migration caused by electrostatic potential, sulfate ions tend to accumulate at approximate 2 mm away from the concrete exposed surface

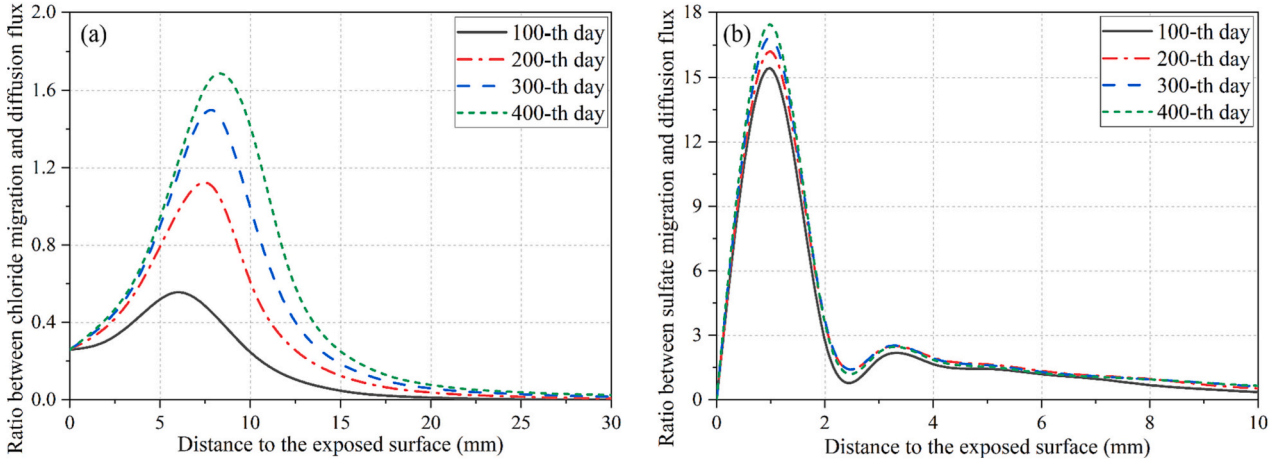


Fig. 19. Flux ratio between ionic migration and ionic diffusion for (a) chloride and (b) sulfate.

leading to a peak value of sulfate ion concentration. The detailed discussion on this feature will be carried out in the next section from the perspective of ionic transport behavior of sulfate ions.

5.2.3. Ionic transport features with electrochemical coupling effect

In order to more clearly distinguish the contribution of multi-ions coupling effect to ionic transport behavior, the two main driving forces of ionic transport under a completely saturated condition, that is, migration and diffusion are compared in terms of ionic flux. The migration flux J_i^m (mol/m^2/s) represents the ionic transport due to the electrostatic potential gradient caused by multi-ions coupling effect, and the diffusion flux J_i^d (mol/m^2/s) represents the ionic transport caused by concentration gradient. Fig. 19 displays the ratios between migration flux and diffusion flux for chloride and sulfate ions respectively.

As for chloride ion, it can be seen from Fig. 19(a) that the flux ratio after 100-day exposure is less than 1, suggesting that the dominant transport behavior is ionic diffusion. This is because at the first 100 day of exposure, the induced electrostatic potential is not large enough, and the corresponding ionic migration does not exceed the contribution of concentration gradient to ionic transport. However, with the increase in exposure duration, the flux ratio gradually becomes larger than 1, which indicates that the ionic migration turns out to be the dominant factor. This feature coincides with the electrostatic potential distribution shown in Fig. 16 in which its value increases over time. Additionally, it can also be found that even after a 400-day exposure to combined chloride-sulfate attack, the maximum flux ratio between ionic migration and diffusion is less than 2.

As for sulfate ion, the flux ratios of various time are plotted in Fig. 19 (b) as a function of concrete cover depth. It can be observed that, compared to that of chloride ion, the flux ratio between migration and diffusion is significantly higher within concrete cover depth of 2 mm. The main reason can be explained from the following two aspects. On the one hand, because sulfate ion is negative divalent (carrying two negative charges), the electrostatic potential has a much more obvious effect on the migration behavior of sulfate ions. On the other hand, due to the relatively smaller diffusion coefficient of sulfate ions, sulfate ions tend to accumulate within 2 mm of concrete cover, which will reduce the concentration gradient in this region and lead to a smaller diffusion flux. Therefore, the increased migration flux in turn leads to a higher concentration of sulfate ion at the cover depth of 2 mm, which agrees well with concentration results shown in Fig. 18. Moreover, it can be found that variation of flux ratio with time is less obvious, which is mainly attributed to the smaller diffusion coefficient and limited diffusion depth of sulfate ions.

5.2.4. Competitive binding intensity under electrochemical coupling

Fig. 20 illustrates the influence of the competitive binding relationship in terms of both free and bound chloride concentration after 400-day exposure. Label M represents cases considering multi-ion coupling, and N represents cases taking the electric neutrality assumption, C represents exposure in single chloride solution, and SC represents exposure in composite solution of sulfate and chloride ions. It can be seen from Fig. 20(a) and (b) that the multi-ions coupling can results in a larger net free chloride concentration, which suggests that considering the interaction among various ionic species can result in a more significant competitive mechanism between chloride and sulfate ions. The main reason can be attributed to the positive electrostatic potential induced by the intrinsic charge imbalance in concrete pore solution, and

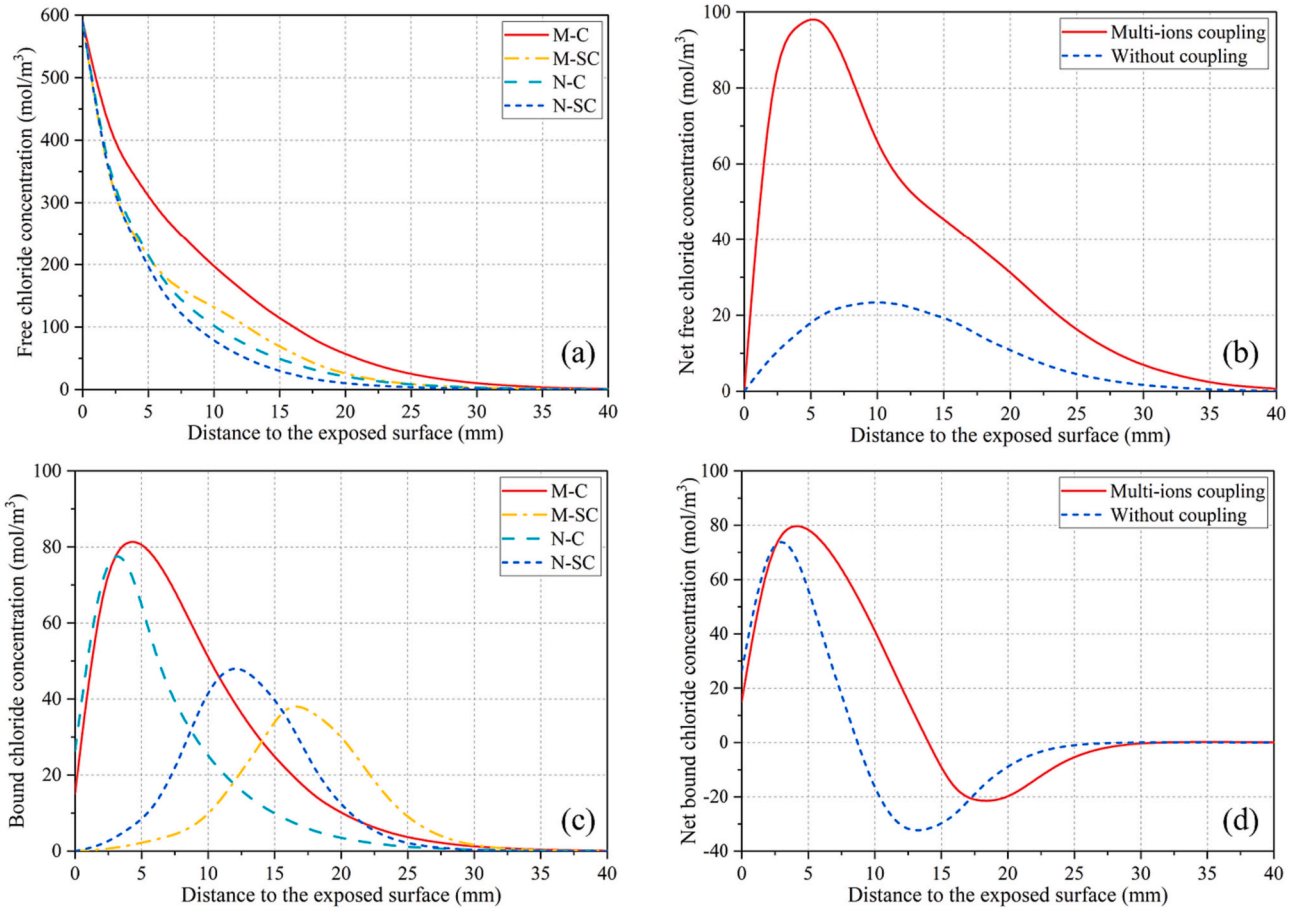


Fig. 20. Influence of multi-ions coupling effect on (a) free chloride concentration; (b) net free chloride concentration; (c) bound chloride concentration; (d) net bound chloride concentration at various concrete depths.

anions such as chloride and sulfate ions can have higher concentrations at the same depth, which in turn lead to a more intense competitive mechanism.

Fig. 20(c) and (d) display the bound chloride concentration and net bound chloride concentrations for both combined attack and single chloride attack with and without the consideration of multi-ions coupling. It can be observed that for concrete exposed to single chloride solution, multi-ions coupling effect will lead to a higher bound chloride concentration. However, as for concrete exposed to composite solution, it can be seen that the bound chloride concentration by considering multi-ionic interaction is smaller than that with the electric neutrality assumption. This is because the multi-ions coupling will also facilitate the ingress of sulfate ions, which will further reduce the binding capacity of cement matrix. Therefore, the maximum value of bound chloride concentration for cases taking multi-ions coupling effect into account is less than that that taking the electric neutrality hypothesis. In addition, it can be found that net bound chloride concentration is higher when considering the interaction of multi-ions, indicating a more intense competitive mechanism. However, it is also observed that a more negative value appears when neglecting multi-ions coupling, which can be explained from the following two aspects. On the one hand, without the ionic migration caused by electrostatic potential, the bound chloride concentration for single chloride attack is smaller. On the other hand, neglecting multi-ions coupling effect will leads to a lower content of sulfate ions in the same depth of concrete cover, that is, the reduced binding capacity caused by sulfate ions is less intense, which makes the bound chloride concentration for combined attack larger. Consequently, the negative peak value is smaller (larger in absolute value) compared to the case considering multi-ions coupling effect.

6. Conclusions

This study presents a comprehensive numerical study for the combined chloride-sulfate attack in cementitious materials. The chemical and electrochemical coupling phenomena: coupled solid-liquid chemical reactions and electrostatic multi-ion coupling effect, during the dual attack of chloride and sulfate ions have been investigated. The chemical reactions among chloride ions, sulfate ions, calcium ions, and hydrated cement compounds are quantitively characterized to reflect the coupling effects. In addition, the evolution of porosity caused by both secondary precipitation of solid products due to the ingress of external ions and internal calcium leaching is considered. According to the chemical coupling, potential influencing factors for the competitive binding intensity between chloride and sulfate ions are compared in detail. Based on the electrochemistry law, the electrostatic coupling among various ionic species can be correspondingly derived, and its effect on ionic transport behavior and the chemical coupling mechanisms are investigated for the first time in literatures. In conclusion, major contributions and findings can be summarized as follows.

1) Compared to the single chloride attack, the combined chloride-sulfate attack can release previously bound chloride ions (due to competitive binding) and shift the position of maximum content of bound chlorides deeper into concrete cover. The combined attack can also lead to a deeper calcium leaching front at approximately 17.5 mm after 400-day exposure. The formation of Friedel's salt (due to Cl^- ingress alone) contributes less in filling of capillary pores, than observed in the combined chloride-sulfate attack, due to precipitation of secondary sulfate hydrates. Due to calcium leaching, an increase in porosity near concrete exposure surface can also be observed even under the existence of external sulfate attack.
2) The influence of buffer coefficient "*f*" characterizing the volume capacity to accommodate expansive products without generating stress is dependent on the calcium aluminate phase content of the cementitious system. For cement with higher amount of calcium aluminates, the decrease of reaction depth and solid products content are more obvious with the increase of buffer coefficient, while for sulfate resisting cement with less calcium aluminates, the results are less sensitive to the change of buffer coefficient.
3) The intensity of the competitive binding relationship between chloride and sulfate ions increases with increase in calcium aluminates content and water-to-cement ratio (which, besides a faster chloride ingress, also increase the binding capacity). Higher external sulfate concentration also aggravates the competitive degree, but the magnitude of the increase and the depth of the impact are relatively much smaller compared to former two factors.
4) The electrostatic potential (along concrete cover depth) induced by the charge imbalance gradually increases with diffusion time. Neglecting electrostatic multi-ionic coupling effect will lead to an underestimated prediction for both chloride and sulfate concentrations. The multi-ions coupling effect has stronger impact on sulfate ions ingress, but due to its lower diffusion coefficient, the most significant impact range is within 2 mm of concrete surface.
5) The electrostatic coupling effect results in a higher content of bound chloride concentration for single chloride attack, while a lower binding capacity is witnessed for the combined attack, which suggests a more competitive situation for chemical binding reactions. Contrary considering both chemical and electrochemical coupling effects, neglecting the electrostatic multi-ionic coupling effect can cause an underestimated chemical coupling strength and lower competitive binding intensity between chloride and sulfate ions.

This work focuses on the combined mechanism between chloride and sulfate ions attack, as well as the inherent coupling effect of multi-ionic species, both demonstrated to play a non-negligible contribution in numerical prediction. However, limitations still exist and special cares could be given to the following aspects when conducting studies in the future. Firstly, the unsaturated condition and even drying-wetting cycles should be further taken into account to more realistically reflect the degradation process in real cases. Secondly, chemical equilibriums and solid-liquid solubilities commonly reported for cementitious materials (full thermodynamic non-ideal description) can be taken into account to more comprehensively characterize the complexity in pore solution, but only at expense of huge increase in computational cost. Besides, with the coexistence of other types of cations in the external solution (e.g., magnesium ions), the competitive binding mechanism and interaction with the cementitious system should be investigated. Finally, the present mesoscopic model mainly focuses on the competitive binding and electrostatic coupling effect, leaving the volume stability during combined chloride-sulfate attack not included, a detailed investigation on the potential influence by adopting the crystallization pressure approach should be conducted.

CRediT authorship contribution statement

Zhaoheng Meng: Conceptualization, Methodology, Software, Validation, Data curation, Writing – original draft, Writing - reviewing & editing.

Qing-feng Liu: Conceptualization, Methodology, Writing - review & editing, Supervision, Project administration, Funding acquisition, Resources.

Neven Ukrainczyk: Conceptualization, Investigation, Writing - reviewing & editing.

Song Mu: Validation, Data curation, Writing - reviewing & editing.

Yufei Zhang: Software, Formal analysis, Visualization.

Geert De Schutter: Writing - reviewing & editing, Resources.

Declaration of competing interest

We declare that we have no financial or personal relationships with other people or organizations that can inappropriately influence our work. There is no professional or other personal interest of any nature or

kind in any product, service and/or company that could be construed as influencing the position presented in, or the review of, the manuscript entitled “Numerical study on the chemical and electrochemical coupling mechanisms for concrete under combined chloride-sulfate attack”.

Data availability

The data that has been used is confidential.

Acknowledgements

This work was funded by the National Natural Science Foundation of China [52222805, 51978396], the Natural Science Foundation of Shanghai, China [22ZR1431400], and the Oceanic Interdisciplinary Program of Shanghai Jiao Tong University, China [SL2021MS016]. Special thanks also go to Dr. Pietro Lura who gave insightful discussions and suggestions during the construction of this work.

References

[1] Q.-f. Liu, Progress and research challenges in concrete durability: ionic transport, electrochemical rehabilitation and service life prediction, RILEM Tech. Lett. 7 (2022) 98–111.
[2] N. Ukrainczyk, T. Matusinovic, Thermal properties of hydrating calcium aluminate cement pastes, Cem. Concr. Res. 40 (2010) 128–136.
[3] Y.X. Cai, Q.F. Liu, L.W. Yu, Z.Z. Meng, Z. Hu, Q. Yuan, B. Savija, An experimental and numerical investigation of coarse aggregate settlement in fresh concrete under vibration, Cement Concrete Compos. 122 (2021), 104153.
[4] M. Saillio, V. Baroghel-Bouny, S. Pradelle, M. Bertin, J. Vincent, J.B.D. de Lacaillerie, Effect of supplementary cementitious materials on carbonation of cement pastes, Cem. Concr. Res. 142 (2021), 106358.
[5] T. Ikumi, I. Segura, Numerical assessment of external sulfate attack in concrete structures. A review, Cem. Concr. Res. 121 (2019) 91–105.
[6] G. De Schutter, K. Audenaert, Evaluation of water absorption of concrete as a measure for resistance against carbonation and chloride migration, Mater. Struct. 37 (2004) 591–596.
[7] J. Shi, J.G. Zhao, H. Chen, P.K. Hou, S. Kawashima, J.H. Qin, X.M. Zhou, J.S. Qian, X. Cheng, Sulfuric acid-resistance performances of magnesium phosphate cements: macro-properties, mineralogy and microstructure evolutions, Cem. Concr. Res. 157 (2022), 106830.
[8] M. Ashraf, M.F. Iqbal, M. Rauf, et al., Developing a sustainable concrete incorporating bentonite clay and silica fume: mechanical and durability performance, J. Clean. Prod. 337 (2022), 130315.
[9] B. Pradhan, Corrosion behavior of steel reinforcement in concrete exposed to composite chloride-sulfate environment, Construct. Build Mater. 72 (2014) 398–410.
[10] F. Xu, Z.Q. Yang, W.Q. Liu, S.G. Wang, H.G. Zhang, Experimental investigation on the effect of sulfate attack on chloride diffusivity of cracked concrete subjected to composite solution, Construct. Build Mater. 237 (2020), 117643.
[11] U.M. Angst, Challenges and opportunities in corrosion of steel in concrete, Mater. Struct. 51 (2018) 1–20.
[12] L.Y. Tong, Q.X. Xiong, M.Z. Zhang, et al., Multi-scale modelling and statistical analysis of heterogeneous characteristics effect on chloride transport properties in concrete, Construct. Build Mater. 367 (2023), 130096.
[13] X.X. Wang, J.P. Liu, Z.Q. Jin, F.X. Chen, P.H. Zhong, L. Zhang, Real-time strain monitoring of reinforced concrete under the attacks of sulphate and chloride ions based on XCT and DIC methods, Cement Concrete Compos. 125 (2022), 104314.
[14] U. Angst, B. Elsener, C.K. Larsen, O. Vennesland, Critical chloride content in reinforced concrete - a review, Cem. Concr. Res. 39 (2009) 1122–1138.
[15] B. Savija, M. Lukovic, E. Schlangen, Lattice modeling of rapid chloride migration in concrete, Cem. Concr. Res. 61-62 (2014) 49–63.
[16] Q.F. Liu, Y.X. Cai, H. Peng, Z.Z. Meng, S. Mundra, A. Castel, A numerical study on chloride transport in alkali-activated fly ash/slag concretes, Cem. Concr. Res. 166 (2023), 107094.
[17] J. Ozbolt, G. Balabanic, M. Kuster, 3D numerical modelling of steel corrosion in concrete structures, Corros. Sci. 53 (2011) 4166–4177.
[18] A. Jamali, U. Angst, B. Adey, B. Elsener, Modeling of corrosion-induced concrete cover cracking: a critical analysis, Construct. Build Mater. 42 (2013) 225–237.
[19] L.-y. Tong, Q.X. Xiong, Z. Zhang, et al., A novel lattice model to predict chloride diffusion coefficient of unsaturated cementitious materials based on multi-typed pore structure characteristics, Cem. Concr. Res. 175 (2024), 107351.
[20] C. Gunasekara, D. Law, S. Bhuiyan, S. Setunge, L. Ward, Chloride induced corrosion in different fly ash based geopolymer concretes, Construct. Build Mater. 200 (2019) 502–513.
[21] K. Pasupathy, J. Sanjayan, P. Rajeev, D.W. Law, The effect of chloride ingress in reinforced geopolymer concrete exposed in the marine environment, J. Build. Eng. 39 (2021), 102281.
[22] C. Alonso, C. Andrade, J. Rodriguez, J.M. Diez, Factors controlling cracking of concrete affected by reinforcement corrosion, Mater. Struct. 31 (1998) 435–441.
[23] B. Savija, J. Pacheco, E. Schlangen, Lattice modeling of chloride diffusion in sound and cracked concrete, Cement Concrete Compos. 42 (2013) 30–40.
[24] Q.F. Liu, Z. Hu, X.E. Wang, H. Zhao, K. Qian, L.J. Li, Z. Meng, Numerical study on cracking and its effect on chloride transport in concrete subjected to external load, Construct. Build Mater. 325 (2022), 126797.
[25] A. Neville, The confused world of sulfate attack on concrete, Cem. Concr. Res. 34 (2004) 1275–1296.
[26] S.U. Al-Dulaijan, M. Maslehuddin, M.M. Al-Zahrani, A.M. Sharif, M. Shameem, M. Ibrahim, Sulfate resistance of plain and blended cements exposed to varying concentrations of sodium sulfate, Cement Concrete Compos. 25 (2003) 429–437.
[27] Y.G. Yu, W. Gao, A. Castel, A.R. Liu, X.J. Chen, M.Y. Liu, Assessing external sulfate attack on thin-shell artificial reef structures under uncertainty, Ocean Eng. 207 (2020), 107397.
[28] Y.J. Chen, J.M. Gao, L.P. Tang, X.H. Li, Resistance of concrete against combined attack of chloride and sulfate under drying-wetting cycles, Construct. Build Mater. 106 (2016) 650–658.
[29] Q.X. Xiong, Q.F. Liu, X.J. Zhang, C. Chen, Chloride diffusion prediction in concrete through mathematical models based on time–dependent diffusion coefficient and surface chloride concentration, J. Mater. Civ. Eng. 34 (2022) 04022309.
[30] Y.G. Yu, Y.X. Zhang, A. Khennane, Numerical modelling of degradation of cement-based materials under leaching and external sulfate attack, Comput. Struct. 158 (2015) 1–14.
[31] S. Sarkar, S. Mahadevan, J.C.L. Meeussen, H. van der Sloot, D.S. Kosson, Sensitivity analysis of damage in cement materials under sulfate attack and calcium leaching, J. Mater. Civ. Eng. 24 (2012) 430–440.
[32] G. Schutter, Quantification of the influence of cracks in concrete structures on carbonation and chloride penetration, Mag. Concrete Res. 51 (1999) 427–435.
[33] H.A.F. Dehwah, M. Maslehuddin, S.A. Austin, Long-term effect of sulfate ions and associated cation type on chloride-induced reinforcement corrosion in Portland cement concretes, Cement Concrete Compos. 24 (2002) 17–25.
[34] F. Shaheen, B. Pradhan, Influence of sulfate ion and associated cation type on steel reinforcement corrosion in concrete powder aqueous solution in the presence of chloride ions, Cem. Concr. Res. 91 (2017) 73–86.
[35] Z. Jin, W. Sun, Y. Zhang, J. Jiang, J. Lai, Interaction between sulfate and chloride solution attack of concretes with and without fly ash, Cem. Concr. Res. 37 (2007) 1223–1232.
[36] M.H. Zhang, J.K. Chen, Y.F. Lv, D.J. Wang, J. Ye, Study on the expansion of concrete under attack of sulfate and sulfate-chloride ions, Construct. Build Mater. 39 (2013) 26–32.
[37] P.W. Brown, S. Badger, The distributions of bound sulfates and chlorides in concrete subjected to mixed NaCl, MgSO4, Na2SO4 attack, Cem. Concr. Res. 30 (2000) 1535–1542.
[38] Y.Z. Cao, L.P. Guo, B. Chen, Influence of sulfate on the chloride diffusion mechanism in mortar, Construct. Build Mater. 197 (2019) 398–405.
[39] G.W. Zhao, J.P. Li, M. Shi, J.F. Cui, F. Xie, Degradation of cast-in-situ concrete subjected to sulphate-chloride combined attack, Construct. Build Mater. 241 (2020), 117995.
[40] J.H. Wang, G.C. Cai, Q. Wu, Basic mechanical behaviours and deterioration mechanism of RC beams under chloride-sulphate environment, Construct. Build Mater. 160 (2018) 450–461.
[41] P.J. Tumidajski, G.W. Chan, K.E. Philipose, An effective diffusivity for sulfate transport into concrete, Cem. Concr. Res. 25 (1995) 1159–1163.
[42] R. Tixier, B. Mobasher, Modeling of damage in cement-based materials subjected to external sulfate attack. I: formulation, J. Mater. Civ. Eng. 15 (2003) 305–313.
[43] J. Marchand, E. Samson, Y. Maltais, J.J. Beaudoin, Theoretical analysis of the effect of weak sodium sulfate solutions on the durability of concrete, Cement Concrete Compos. 24 (2002) 317–329.
[44] E. Samson, J. Marchand, Modeling the transport of ions in unsaturated cement-based materials, Comput. Struct. 85 (2007) 1740–1756.
[45] Z.Z. Meng, Y.F. Zhang, W.K. Chen, C.Q. Fu, Q.X. Xiong, C.L. Zhang, Q.F. Liu, A numerical study of moisture and ionic transport in unsaturated concrete by considering multi-ions coupling effect, Transp. Porous Media (2023), https://doi.org/10.1007/s11242-023-02011-6.
[46] S.S. Qin, D.J. Zou, T.J. Liu, A. Jivkov, A chemo-transport-damage model for concrete under external sulfate attack, Cem. Concr. Res. 132 (2020), 106048.
[47] C.L. Zhang, W.K. Chen, S. Mu, B. Savija, Q.F. Liu, Numerical investigation of external sulfate attack and its effect on chloride binding and diffusion in concrete, Construct. Build Mater. 285 (2021), 132913.
[48] P.G. Wang, R. Mo, S. Li, J. Xu, Z.Q. Jin, T.J. Zhao, D.Z. Wang, A chemo-damage-transport model for chloride ions diffusion in cement-based materials: combined effects of sulfate attack and temperature, Construct. Build Mater. 288 (2021), 123121.
[49] P.G. Wang, R. Mo, X.M. Zhou, J. Xu, Z.Q. Jin, T.J. Zhao, A chemo-thermo-damage-transport model for concrete subjected to combined chloride-sulfate attack considering the effect of calcium leaching, Construct. Build Mater. 306 (2021), 124918.
[50] Z. Chen, J. Yu, V. Bindiganavile, C. Yi, C. Shi, X. Hu, Time and spatially dependent transient competitive antagonism during the 2-D diffusion-reaction of combined chloride-sulphate attack upon concrete, Cem. Concr. Res. 154 (2022), 106724.
[51] Z. Chen, L.Y. Wu, V. Bindiganavile, C.F. Yi, Coupled models to describe the combined diffusion-reaction behaviour of chloride and sulphate ions in cement-based systems, Construct. Build Mater. 243 (2020), 118232.
[52] B.B. Guo, G.F. Qiao, D.S. Li, J.P. Ou, Multi-species reactive transport modeling of electrochemical corrosion control in saturated concrete structures including electrode reactions and thermodynamic equilibrium, Construct. Build Mater. 278 (2021), 122228.

[53] Y.G. Yu, W. Gao, Y. Feng, A. Castel, X.J. Chen, A.R. Liu, On the competitive antagonism effect in combined chloride-sulfate attack: a numerical exploration, Cem. Concr. Res. 144 (2021), 106406.
[54] Y.G. Yu, X.J. Chen, W. Gao, D. Wu, A. Castel, Modelling non-isothermal chloride ingress in unsaturated cement-based materials, Construct. Build Mater. 217 (2019) 441–455.
[55] Q.F. Liu, M.F. Iqbal, J. Yang, X. Lu, P. Zhang, M. Rauf, Prediction of chloride diffusivity in concrete using artificial neural network: modelling and performance evaluation, Construct. Build Mater. 268 (2021), 121082.
[56] B. Johannesson, Comparison between the Gauss' law method and the zero current method to calculate multi-species ionic diffusion in saturated uncharged porous materials, Comput. Geotech. 37 (2010) 667–677.
[57] D.Z. Wang, X.M. Zhou, Y.F. Meng, Z. Chen, Durability of concrete containing fly ash and silica fume against combined freezing-thawing and sulfate attack, Construct. Build Mater. 147 (2017) 398–406.
[58] A.E. Idiart, C.M. Lopez, I. Carol, Chemo-mechanical analysis of concrete cracking and degradation due to external sulfate attack: a meso-scale model, Cement Concrete Compos. 33 (2011) 411–423.
[59] R. Tixier, Microstructural Development and Sulfate Attack Modeling in Blended Cement-Based Materials, Arizona State University, Ann Arbor, 2000, p. 254.
[60] D.D. Sun, K. Wu, H.S. Shi, L.T. Zhang, L.H. Zhang, Effect of interfacial transition zone on the transport of sulfate ions in concrete, Construct. Build Mater. 192 (2018) 28–37.
[61] V.Q. Tran, A. Soive, V. Baroghel-Bouny, Modelisation of chloride reactive transport in concrete including thermodynamic equilibrium, kinetic control and surface complexation, Cem. Concr. Res. 110 (2018) 70–85.
[62] P.F. Lito, S.P. Cardoso, J.M. Loureiro, C.M. Silva, Ion Exchange Equilibria and Kinetics, Springer, Ion Exchange Technology I, 2012, pp. 51–120.
[63] J. Jain, N. Neithalath, Analysis of calcium leaching behavior of plain and modified cement pastes in pure water, Cement Concrete Compos. 31 (2009) 176–185.
[64] Q.X. Xiong, L.Y. Tong, Z.D. Zhang, C.J. Shi, Q.F. Liu, A new analytical method to predict permeability properties of cementitious mortars: the impacts of pore structure evolutions and relative humidity variations, Cement Concrete Compos. 137 (2023), 104912.
[65] Q.X. Xiong, L.-y. Tong, F. Meftah, et al., Improved predictions of permeability properties in cement-based materials: a comparative study of pore size distribution-based models, Construct. Build Mater. (2023), 133927.
[66] K. Nakarai, T. Ishida, K. Maekawa, Modeling of calcium leaching from cement hydrates coupled with micro-pore formation, J. Adv. Concrete Technol. 4 (2006) 395–407.
[67] Q.F. Liu, X.H. Shen, B. Savija, Z.Z. Meng, D.C.W. Tsang, S. Sepasgozar, E. Schlangen, Numerical study of interactive ingress of calcium leaching, chloride transport and multi-ions coupling in concrete, Cem. Concr. Res. 165 (2023), 107072.
[68] X.N. Li, X.B. Zuo, Y.X. Zou, Modeling and simulation on coupled chloride and calcium diffusion in concrete, Construct. Build Mater. 271 (2021), 121557.
[69] T. Ikumi, S.H.P. Cavalaro, I. Segura, A. Aguado, Alternative methodology to consider damage and expansions in external sulfate attack modeling, Cem. Concr. Res. 63 (2014) 105–116.
[70] R.J. Flatt, G.W. Scherer, Thermodynamics of crystallization stresses in DEF, Cem. Concr. Res. 38 (2008) 325–336.
[71] G.W. Scherer, Stress from crystallization of salt, Cem. Concr. Res. 34 (2004) 1613–1624.
[72] E. Samson, J. Marchand, Modeling the transport of ions in unsaturated cement-based materials, Comput. Struct. 85 (2007) 1740–1756.
[73] H.M. Jennings, P.D. Tennis, Model for the developing microstructure in Portland cement pastes, J. Am. Ceram. Soc. 77 (1994) 3161–3172.
[74] S. Bejaoui, B. Bary, Modeling of the link between microstructure and effective diffusivity of cement pastes using a simplified composite model, Cem. Concr. Res. 37 (2007) 469–480.
[75] S. Igarashi, V. Kawamura, A. Watanabe, Analysis of cement pastes and mortars by a combination of backscatter-based SEM image analysis and calculations based on the powers model, Cement Concrete Compos. 26 (2004) 977–985.
[76] L. Lam, Y.L. Wong, C.S. Poon, Degree of hydration and gel/space ratio of high-volume fly ash/cement systems, Cem. Concr. Res. 30 (2000) 747–756.
[77] I. Pane, W. Hansen, Investigation of blended cement hydration by isothermal calorimetry and thermal analysis, Cem. Concr. Res. 35 (2005) 1155–1164.
[78] L.-y. Tong, Q.-f. Liu, Q.X. Xiong, Z. Meng, O. Amiri, M. Zhang, Modelling the chloride transport in concrete from microstructure generation to chloride diffusivity prediction, Comput.-Aided Civ. Inf. (2024).
[79] S. Sarkar, S. Mahadevan, J.C.L. Meeussen, H. van der Sloot, D.S. Kosson, Numerical simulation of cementitious materials degradation under external sulfate attack, Cement Concrete Compos. 32 (2010) 241–252.
[80] B.H. Oh, S.Y. Jang, Prediction of diffusivity of concrete based on simple analytic equations, Cem. Concr. Res. 34 (2004) 463–480.
[81] Q.F. Liu, D. Easterbrook, J. Yang, L.Y. Li, A three-phase, multi-component ionic transport model for simulation of chloride penetration in concrete, Eng. Struct. 86 (2015) 122–133.
[82] M. Maes, Combined Effects of Chlorides and Sulphates on Cracked and Self-Healing Concrete in Marine Environments, Ghent University, 2015.
[83] Common Portland Cement, Standardization Administration of China: Beijing, China, 2007.
[84] J. Ollivier, J. Maso, B. Bourdette, Interfacial transition zone in concrete, Adv. Cem. Bas. Mat. 2 (1995) 30–38.
[85] L.-X. Mao, Z. Hu, J. Xia, et al., Multi-phase modelling of electrochemical rehabilitation for ASR and chloride affected concrete composites, Compos. Struct. 207 (2019) 176–189.
[86] Y. Cai, Q.-F. Liu, Stability of fresh concrete and its effect on late-age durability of reinforced concrete: an overview, J. Build. Eng. 179 (2023), 107701.
[87] K.S. Wan, Y. Li, W. Sun, Experimental and modelling research of the accelerated calcium leaching of cement paste in ammonium nitrate solution, Construct. Build Mater. 40 (2013) 832–846.
[88] T. Ikumi, S.H.P. Cavalaro, I. Segura, The role of porosity in external sulphate attack, Cement Concrete Compos. 97 (2019) 1–12.
[89] Z. Meng, Q.F. Liu, J. Xia, Y. Cai, X. Zhu, Y. Zhou, L. Pel, Mechanical–transport–chemical modeling of electrochemical repair methods for corrosion-induced cracking in marine concrete, Comput.-Aided Civ. Inf. Eng. 37 (14) (2022) 1854–1874.